People's Democratic Republic of Algeria
Ministry of Higher Education and Scientific

Research

Amar Thelidji- Laghouat University

FACULTY of TECHNOLOGY
MECHANICAL ENGINEERING DEPARTMENT

MASTER MEMORY

Presented by: Tarchid Youcef and Cheriki Idris

DOMAIN: SCIENCES and TECHNOLOGIES.

DEPARTEMENT: MECHANICAL ENGINEERING

OPTION: ENERGETIC

Theme

Numerical simulation of particles concentration in wind tunnel model

Jury Member:	**Grade**	
HACHANI Lakhdar	Professor	President
BEN SAYAH Khaled	MCA	Examiner
HADJ AISSA aissa	MAA	Reporter

2021/2022

ملخص: يُعرَّف نقل الرمل الإيولي بأنه نقل جزيئات الرمل بواسطة الرياح بطرق مختلفة، اعتمادًا بشكل أساسي على سرعة الرياح وحجم وتركيز جزيئات الرمل.

يهدف هذا العمل إلى محاكاة عددية لهذه الظاهرة الطبيعية بالتحديد تأثير سرعة الرياح وتركيز جزيئات الرمال داخل نفق الرياح.

أجريت هذه الدراسة داخل نموذج نفق الرياح ثلاثي الأبعاد وثابت (أي لا تتغير متغيرات المجال بمرور الوقت) باستخدام برنامج "COMSOL Multiphysics" الذي يستخدم نموذج أويلر اولير لتدفق المضطرب والذي يعتمد بدوره على نموذج (k-ε)المضطرب لحل هذا النوع من المحاكاة العددية.

من بين أهم نتائج المتحصل عليها في هذه الدراسة هي العلاقة بين سرعة الرياح وتركيز جزيئات الرمل في نقل الرمل الإيولي.

Abstract: Aeolian sand transport is defined as the transport of sand particles by wind in various ways, mainly depending on the wind speed and the size and concentration of sand particles.

This work aims to numerically simulate this natural phenomenon, specifically the effect of wind speed and the concentration of sand particles inside the wind tunnel.

This study was carried out inside wind tunnel 3D model and Stationary using the "COMSOL Multiphysics" program that uses the Euler Euler turbulent flow model, which in turn depends on the turbulent (k-ε) model to solve this type of numerical simulation.

One of the most important results of this study is the relationship between wind speed and sand particles concentration in the transport of aeolian sand.

Résumé: Le transport de sable éolien est défini comme le transport de particules de sable par le vent de différentes manières, principalement en fonction de la vitesse du vent et de la taille et de la concentration des particules de sable.

Ce travail vise à simuler numériquement ce phénomène naturel, plus précisément l'effet de la vitesse du vent et de la concentration des particules de sable à l'intérieur de la soufflerie.

Cette étude a été réalisée à l'intérieur du modèle 3D de soufflerie et stationnaire à l'aide du programme "COMSOL Multiphysics" qui utilise le modèle d'écoulement turbulent Euler Euler, qui à son tour dépend du modèle turbulent (k-ε) pour résoudre ce type de simulation numérique.

L'un des résultats les plus importants de cette étude est la relation entre la vitesse du vent et la concentration de particules de sable dans le transport du sable éolien.

Dedications

I dedicate this work to my mother and father; you have been and still are the greatest support in my life, to my grandmother in particular and all family members, loved ones and friends in general. Thank you for everything.

Youcef

Dedications

I dedicate this humble work

To the owner of a fragrant biography and enlightened thought, because he had the first credit for reaching higher education (my beloved father), may God prolong his life.

To the one who set me on the path of life, calmed me, and cared for me until I grew up (dear mother)

I dedicate this work to all my friends and those who were with me in the university

And also to everyone who helped me from near or far

Idris

Thanks to

All thanks first to God who gave us the will

To Complete this work

All our infinite gratitude to our promoters:

Dr. HADJ AISSA aissa for his dear supervision and assistance.

We would also like to thank the Head of the Department Youssoufi Ahmed and all the professors of the Department Mechanical engineering who spared no effort in it for sending their knowledge and experience

to the students.

Table des matières

List of Figures

List of table

Nomenclature

SYMBOLES	PARAMETER	UNITE
$\boldsymbol{F_m}$	the interphase momentum transfer term	N/m^3
$\boldsymbol{F_d}$	total drag	N/m^3
$\boldsymbol{p_s}$	The solid pressure.	Pa
$\boldsymbol{p_t}$	The total pressure	Pa
$\boldsymbol{p_s}$	static pressure	Pa
$\boldsymbol{\rho_s}$	the grain density	kg/m^3
$\boldsymbol{\phi_{d,max}}$	maximum packing limit	(dimensionless)
$\boldsymbol{\phi_c}$	Volume fraction of continuous phase	(dimensionless)
$\boldsymbol{\phi_d}$	Volume fraction of dispersed phase	(dimensionless)
$\boldsymbol{\mu_C}$	The continuous phase viscosity	kg/m^3
$\boldsymbol{\mu_D}$	The dispersed phase viscosity	kg/m^3
$\boldsymbol{\mu_T}$	the resulting turbulent viscosity	kg/m^3
$\boldsymbol{\mu_{mix}}$	The mixture viscosity	kg/m^3
$\boldsymbol{F_{drag,d}}$	The drag force dispersed phase	N/m^3
$\boldsymbol{F_{drag,c}}$	The drag force continuous phase	N/m^3
$\boldsymbol{u_{slip}}$	The slip velocity	m/s
$\boldsymbol{u_d}$	Velocity magnitude, Dispersed phase	m/s
$\boldsymbol{u_c}$	Velocity magnitude, Continuous phase	m/s
$\boldsymbol{u_m}$	the mixture velocity	m/s
$\boldsymbol{u^*}$	wind speed	cm/s
$\boldsymbol{\beta}$	The drag force coefficient	(dimensionless)
$\boldsymbol{C_\mu}$	model constant	(dimensionless)

C_D	drag coefficient	(dimensionless)
C_S	shape coefficient	(dimensionless)
p_k	The production term	(dimensionless)
σ_T	Turbulent particle Schmidt number	(dimensionless)
τ_c	The viscous stress tensors for continuous phase	Pa
τ_d	The viscous stress tensors for dispersed phase	Pa
$D_{m,d}$	The turbulent dispersion coefficient	(dimensionless)
Phid	Volume fraction, dispersed phase(concentration)	(dimensionless)
w'	velocity component of the airflow	cm/s
$\bar{u}$,$\bar{v}$,and $\bar{w}$	The mean velocities	cm/s
u', v', and w'	The eddy velocity	cm/s
$w_1$and w_2	The initial and final vertical velocities	cm/s
$u_1$and u_2	The initial and final horizontal velocities	cm/s
w_f	quartz spheres of different sizes	cm/s
w_{fn}	natural quartz grains	cm/s

Greek symbols

ρ	The density of the fluid	kg/m^3
u	Velocity of each phase	m/s
ϕ	The phase volume fraction	(dimensionless)
p	Mixture pressure	Pa
τ	The viscous stress tensor for each phase	Pa
g	Gravitational acceleration	m/s^2
F	Volume force term	N/m^3

W	The force resulting from the static pressure	N/m^3
μ	The dynamic viscosity of the respective phase.	Pa·s
k	The kinetic energy	m^2/s^2
ε	The dissipation rate of turbulent kinetic energy	m^2/s^3
z	Height	m
h	Maen Height of saltation	cm
d	diameter	mm
A	Constant	(dimensionless)
h and ℓ	The maximum jump height and jump lengths	m
$\boldsymbol{\alpha}$	The impact angle	Degree
A and S	The stagnation point and S the separation points	(dimensionless)
t	The time taken to complete the trajectory	s

Dimensionless groups

Re	Reynolds number
k-ε	turbulence model

LIST OF ABBREVIATIONS

NAL: National Aerospace Laboratory of Japan.

3D: Three Dimensional.

2D: Two Dimensional.

CAD: Computer-Aided Design.

CFD: Computational Fluid Dynamics.

r.p.s: Round per second.

RANS: Reynolds-Averaged Navier-Stokes.

TKE: The turbulence kinetic energy

GENERAL INTRODUCTION

For many centuries, fluid flow researchers have studied fluid flow in different ways. Flow is still an important area of research especially in areas where flow plays an important role. Gas flows are studied for the development of cars, aircraft and spacecraft. As well as the design of machines such as turbines combustion engines and many other fields.

In our topic, we will deal with the flow of fluids in nature specifically the transport of Aeolian sands.

The process of transporting sand by wind is called the Aeolian process. It refers to the movement of sand particles. This occurs in deserts, beaches, and other areas with little vegetation cover. Such as dry lake bottoms.

The terms "sand and dust" refer to the solid and very small particles that arise from the weathering of rocks.where sand is defined as mineral particles with diameters ranging from 63 to 500 µm. As for dust. It is particles less than 63 µm in diameter. Aeolian sand transportation depends on:

Wind speed direction and duration as well as sand formation (particle size and distribution) without forgetting the natural conditions (vegetation cover, erosion of rocks, and height of sand dunes humidity).

In this work, we relied on a 5m x 1m x 1m rectangular wind tunnel (length, width and height, respectively) with a specific concentration of sand particles inside.

The aim of this work is to simulate the concentration of sand particles inside a wind tunnel. In our study, we relied on the "COMSOL Multiphysics ®" program by exploiting the turbulent Euler–Euler model, which in turn uses the turbulent (k-ε) model and solve this form of study.

The memory sections mainly consists of three chapters:

The first chapter is mainly based on a general introduction to the Aeolian transport of sand particles in nature (Aeolian Transport Modes, Suspension and Saltation). We also talked about the wind tunnel (History, Definition and Types) which is the tool used in this study.

The second chapter mainly focuses on the equations that govern the process and that must be solved during the study (Navier-Stokes equations, The Euler-Euler Model Equations, Mass Balance, Momentum Balance, Inter Phase Momentum Transfer, and Turbulent Two-Phase Flow Modelling.)

In the third chapter: geometric figure, configuration and the mesh. For wind tunnel and its characteristics.

We also discussed the results in which we focused on the effects and behavior of Velocity magnitude, continuous phase $\boldsymbol{u_c}$ (m/s) and dispersed phase $\boldsymbol{u_d}$ (m/s), sand particles concentration(Volume fraction, dispersed phase (Phid)) within the tunnel.

All this in order to give a clear indication about the movement and mobility of Aeolian sand particles in nature.

Chapter I : GENERALITY

I.1 INTRODUCTION

The transport of granular materials by turbulent air is an important topic for various purposes. The way sand is eroded, moved and deposited by wind is an aeolian process.

The first thing that is moved by the wind is sand particles whose diameter is from 63–500 μm then these particles bounce along the surface in a series of jumps known as salt. These particles can move a group of objects. [Greeley and Iversen.1985; Shao, 2000].

Dust particles are those with a diameter less than 63 μm [Greeley and Iversen.1985]. Dust particles are moved upwards by convection and turbulent vortices. Particles with a diameter of more than 500 may roll or slide along the surface under the influence of salt particles and wind pressure, and this is known as creep [Bagnold,1941]. In order to study the movement of these molecules, numerical simulation is necessary. It is the most appropriate way for this in our time. This is only done in the wind tunnel, which is a way to study air fluctuations. [Kok, Jasper F., and Nilton O. Renno. (2009)].

I.2 WIND TUNNEL

I.2.1 History

Discovery and development through experimental means is his lifeblood, dating back to George Kelly. In 1804, he built a vortex arm device to test wings. It is just a lifting surface (airfoil) installed at the end of a long road, which rotates at a certain speed to create airflow on the air foil. In modern aerospace engineering, the workhorse of such experiments is the wind tunnel, so much so that today most aerospace industry, government and university laboratories have a full range of wind tunnels from low subsonic to hypersonic [YANG, NKOOC.(2012)]

Then, with development, it is necessary to consider the physical aspects and consider the cost of building the wind tunnel. With this in mind, NAL produced its first high-spec computer in 1987, marking the beginning of fully digital simulation and paralleling the development of Computational Fluid Dynamics (CFD) codes. Like multi-block euler symbols by Sawada. [K. Sawada et al (1987)]. Applied to 3D viscosity analysis of aircraft wings. These were the first major achievements of computers.

In 1993, the second generation of the same product NAL appeared, and the supercomputer became the basic system for numerical simulation. [Y. Matsuo et al (2010)]

In 2002, NAL introduced the most efficient third generation product for building digital antenna tunnels. After that, especially in 2008, a new project appeared, Numerical Wind tunnel (NWT). Tunnel project, with very high efficiency and quality. In short, this is the history of the discovery and development of wind tunnels; especially digital wind tunnels [Y. Matsuo et al (2017)]

I.2.2 Wind tunnel

A wind tunnel is a facility for conducting aerodynamic experiments. Internally, airflow can be generated while maintaining adjustable parameters such as speed, pressure and temperature. The subject is placed in it and experiments are performed to understand how it behaves in this state, with specific sensors measuring the forces and pressures acting on the body. Despite advances in computational flow simulation, wind tunnels are still used to obtain experimental information that can help solve aerodynamic problems. The main reason is that the Navier-Stokes equations, the fundamental equations of aerodynamics, do not have exact analytical solutions.

Approximate solutions can be obtained with CFD but they do not have accuracy since the starting point of them is a simplified model therefore it is better to realize experimental studies too. Wind tunnels make it possible to use models that can be prepared early in design cycles, they include the full complexity of real fluid flow, and they can provide large amounts of reliable data, therefore they are the most rapid, economical, and accurate means for conducting aerodynamic research and obtaining aerodynamic data to support design decisions. [Edoardo Foschi. (2020)].

The wind tunnel provides great benefits for aerodynamic tests compared to free flight testing, that is:

- Specified flow condition such as Mach number and incidence can be achieved sustained much easier in a wind tunnel.
- Dangerous, uncontrollable flight condition may safely investigate in wind tunnel.
- Data acquisition and processing is simpler with direct connection to ground based equipment.

The main disadvantage of wind tunnel is that it is seldom possible to reproduce the condition of full-scale motion exactly. This is mainly due to the use of scaled models for reason of tunnel cost and power consumption. [YANG, NKOOC. (2012)]

Figure (I - 1): Wind tunnel design [www.edibon.com/en/computer-controlled-aerodynamic-tunnel-300-x-300-mm]

I.2.3 Tunnel Geometry

Wind tunnel geometry is one of the important factors in wind tunnel classification. In fact, the wind tunnel geometry can be divided into two parts, an open-loop wind tunnel and a closed-loop wind tunnel. As shown in (Fig (I - 2)) in an open-circuit wind tunnel, the air leaving the diffuser is not recirculated back into the next cycle that generates airflow but the air drawn from the constricting cone is fresh from ambient air. Air is not compressed or heated. Tom Benson (2009) said: "A wind tunnel that is open at both ends and pulls air from the room into the test track is called an open back wind tunnel". The advantage of an open-loop wind tunnel is reduced construction costs, as no heat exchangers are required for the next flow cycle. Also less material is used because no channel structure is required to connect the tunnel's diffuser to its constricted cone. As for the closed-loop wind tunnel, as shown in (Fig (I - 3)) the geometry is quite different from the open-loop wind tunnel. A closed loop, or closed downwind duct requires a duct design to connect the diffuser back to the inlet of the constricting cone. In this tunnel design, a heat exchanger is required to reduce the air temperature so that it can be reused in the next flow generation cycle after the air temperature has risen slightly after being compressed by the fan. . [Bahari, Muhammad Adnin Mat, 2012]

I.2.4 CLASSIFICATION OF WIND TUNNEL

There are great deals of way to classify the wind tunnel. Several types of wind tunnel have been invented for various functions toward the study of aerodynamic. The variously types of wind tunnel are actually the evolution of the subsonic wind tunnel. Then the existence of other wind tunnel starts to take place in aerodynamic research. Basically, the wind tunnel can be classified by its speed regime tunnel geometry and the working fluid in the tunnel.

a) Based on speed range

The most appropriate classification of wind tunnels is by the speed range they cover. The classification of wind tunnels based on the speed range includes:

- **Low speed wind tunnel**

The flow velocity in low subsonic wind tunnel is of the Mach number range of zero till 0.3. Viscous and inertial forces are dominant while compressibility effects are negligible.

- **High speed wind tunnel**

The designation high speed usually includes high subsonic, transonic and low supersonic regimes, so that the range of the flow velocity for high speed wind tunnel is of Mach number between 0.3 and 1.4. Here, in principle, compressibility effects are of dominant importance. However, viscous effects also play an important part in particular when shock boundary layer intersection leads to flow separation.

- **Supersonic wind tunnel**

The flow velocity in supersonic wind tunnel is the range of Mach number of 1.4 till 5.0. Compressibility effects are dominant. The pressure disturbance raises in the flow field propagating downstream.

- **Hypersonic wind tunnel**

The flow velocity in hypersonic wind tunnel is of Mach number above 5.0. It is desired to allow real gas effects to occur. This requires that besides the high Mach number in test section also high total temperatures are provided. The high temperatures, which are linked with high pressures, yield vibration of the gas molecules, possibly causing dissociation and ionization. These are dominant features of hypersonic flows where the gas can no longer be treated as an ideal gas.

With increasing Mach number, the tendency to intermittent operating wind tunnels linked with an appropriate energy storage arrangement, becomes more and more compelling. However, for measurement of low subsonic flow, the continuously operating wind tunnel is more preferred. [YANG, NKOOC. (2012)]

b) Based on flow circulation

The other wind tunnel classification based on flow circulation is divided into open circuit wind tunnel and closed-circuit wind tunnel.

- **Open loop wind tunnel**

Open circuit wind tunnel is first type of wind tunnel built. The tunnel is usually referred to as an Eiffel type. Such a wind tunnel consists of a nozzle, at test section, a diffuser and a driving unit. The principle work of this wind tunnel is a direct sucking of the atmospheric air lying outside of the wind tunnel brought into the tunnel settling chamber and continued to the end of the wind tunnel using a driving unit then the air is throwing away to atmosphere. The position of driving units can be at the downstream end where the tunnel is operated as suction tunnel while otherwise it would be termed a blow down tunnel. The suction tunnel is more preferred in a design by a reason of airflow quality.

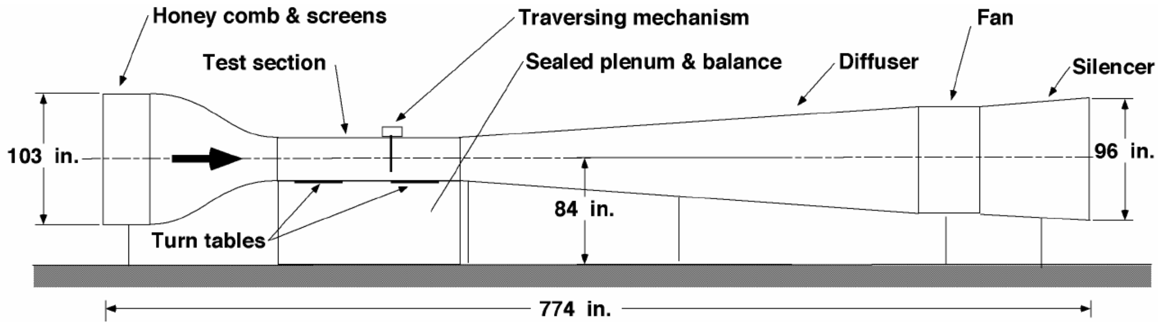

Figure (I - 2): Open loop wind tunnel. [flight.engr.ucdavis.edu/facilities/aeronautical-wind-tunnel/]

- **Closed loop wind tunnel**

Closed loop wind tunnel has been developed to reduce the amount of used energy. This tunnel is also called as Gottingen type. The principle work of this tunnel is by circulating the used airflow passing by the diffuser to the settling chamber using the connecting channel. The closed-circuit tunnel consists of three types including single and double return. Of these, only the first is in general acceptance at present. In the double return arrangement, the particular air that scrapes along the wall of the return passages forms wakes in the centre of the jet and hence passes directly over the model. Unless the contraction ratio is large, this air is extremely tuber lent and tends to make the interpretation of the test data difficult. The fans are preferred attach on the connecting channel by reason of a protection from the model failure and of good from standpoint of fan [YANG, NKOOC. (2012)]

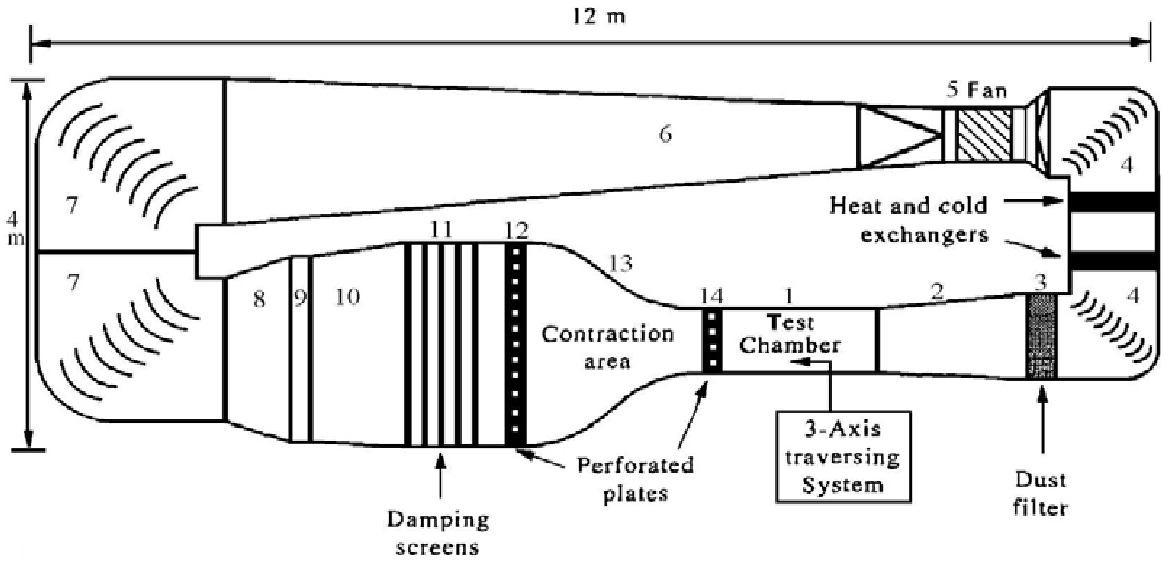

Figure (I - 3): Closed loop wind tunnel. [Di Clemente, M. et al.]

I.3 Transport of Particles by the Wind

The transport of particles by wind can occur in different ways, mainly depending on particle size and wind speed. As the wind speed increases, sand particles with a diameter of about 100 µm are first moved by liquid resistance. Once lifted, the particles bounce along the surface in a process called jumping. The impact of these hoppers on the surface can move particles of various sizes. Very small particles are effectively ejected from the ground by the influence of the salted particles. After ejection, dust particles are prone to turbulent fluctuations, so they are usually suspended for a short or long term.

The effects of salted particles can also mobilize other particles. However, the acceleration of particles larger than about 500 µm in diameter is severely limited by their high inertia, and these particles generally do not form salts. Instead, they return to the ground after a brief bounce (<10mm), usually in a form of transport known as crawling. Alternatively, larger particles may roll or slide along the surface, driven by the impact and drag of the salted particles, in a transport mode called creep. Creeping and creeping can account for a significant portion of the total wind sand flow. The transport of particles by wind can be roughly divided into several physical states (Fig (I - 4)):

- Long-term suspension (< 20 µm),

- Short-term suspension (20 – 70 µm),
- Transitions (70 – 500 µm)
- Creep and creep (> 500 µm). [Van Rijn, Leo C. (2018)].

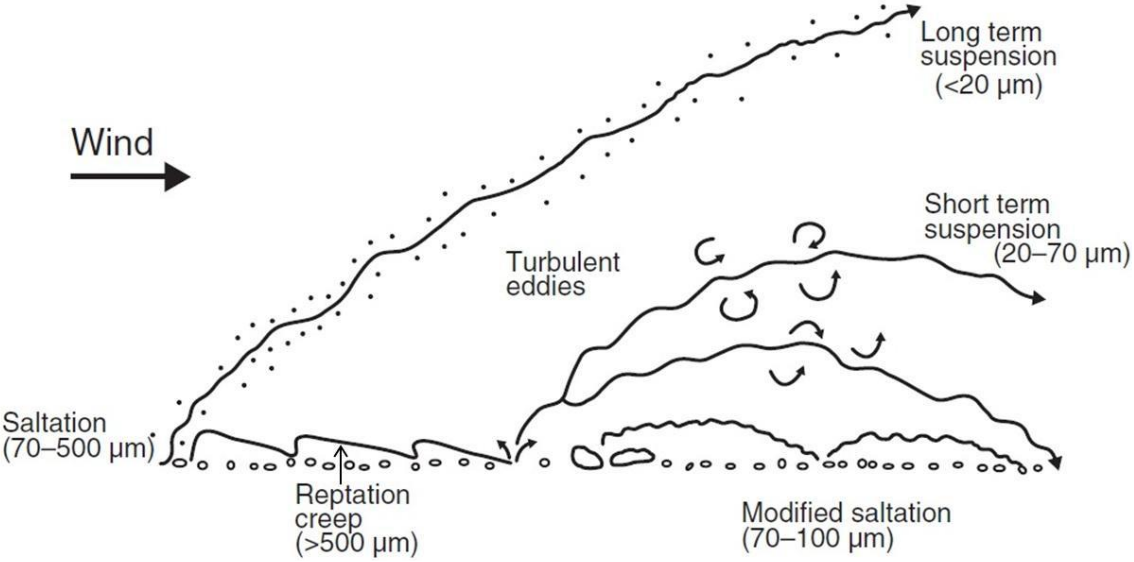

Figure (I - 4): Modes of wind-blown transport of sediment (Kok et al., 2012)

I.3.1 Aeolian Transport Modes

Different types of particle transport are defined by wind speed and particle size. Boulders are grains that move very close to the bed. This pattern includes hopping, in which the grain moves forward through a series of hops, and surface traction, in which the grain rolls or slides along the surface due to direct fluid resistance or the influence of salted particles. Surface tensile loads are sometimes also called contact loads because the grains do not lose contact with the surface. Other terms used to describe loss of contact with the bed that do not or only occur for a short period of time include surface creep [Greeley & Iversen 1985, p. 293].The second important mode of transport is suspension, in which particles are lifted from the surface and carried over long distances by the flow without re-contacting the bed. Turbulent airflow can keep the grain in suspension if the vertical fluctuating velocity component of the airflow: $w' = w - \overline{w}$ Exceeds the grain's sinking velocity (w_f). The calculated sedimentation velocities of quartz spheres of different sizes and the measured sedimentation velocities of natural quartz particles in air are shown in the figure (Fig (I - 5)). In a neutrally stratified atmosphere, where buoyancy effects due to thermal differences do not play a role [Von Kármán 1937], the distribution of the velocity component of vertical variation near the surface is normally distributed with a mean of 0 and a standard deviation of $\sqrt{\overline{w}'^2}$, which is equal to Au^* where A is a constant. The mean of A *is* in the range 0.7-1.4, with an approximate mean of 1.0; thus $\sqrt{\overline{w'^2}}/\,u^*\approx 1.0$ [Lumley & Panofsky 1964, p. 134]. The ratio w_f/u^* provides a measure of the susceptibility of grains to suspension transport [Francis 1973, Fig. (Fig (I - 6))].

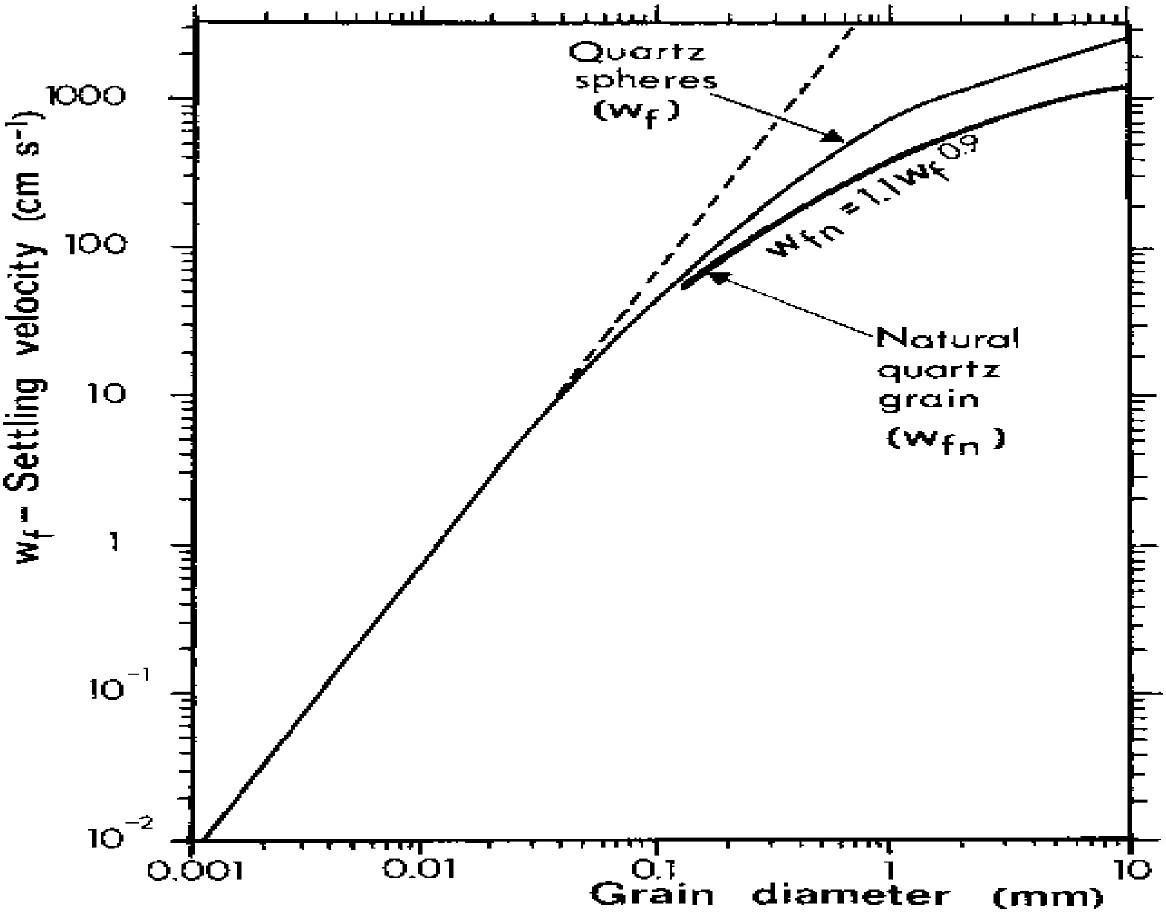

Figure (I - 5): Calculated settling velocities (w_f) of quartz spheres (after von Engelhardt1977) and measured settling velocities (w_{fn}) of natural quartz grains in air (after Cui et al. 1983). The dashed line shows the deviation from Stokes' law for particles larger than 0.04mm

The dividing line for $w_f/u^*= 1$ is arbitrary. There is no clear separation between bed load and suspended load, but rather a gradual transition [Nickling 1983]. Pure bed borne transport occurs when the vertical velocity component associated with turbulence has no significant effect on particle trajectories. This happens when $w_f/u^* \gg 1$. A pure suspension exists when the particle settling velocity is very small relative to the friction velocity ($w_f/u^* \ll 1$). When w_f/u^*takes values close to 1, the particles move in a modified jumping motion [Hunt & Nalpanis 1985, Nalpanis 1985], in which they show random trajectories with fluid transitions between jumping and levitating. An arbitrary boundary between pure and modified salting theoretically determined by Nalpanis (1985) is shown in (Fig (I - 6)). It roughly corresponds to the value of w_f/u^*= 1.25, which Bagnold (1973) considers to be the point at which the solid particles are suspended.

The upper limit of pure suspension can be assumed to be $w_f/u^*\approx$ 0.7. [Gillette et al. 1974]. The sediment logical significance of distinguishing bed-loaded and suspended-loaded is the distance the particles are carried by the wind. Particles 0.1–0.3 mm in diameter are most susceptible to salinization during typical storms, forming dunes, while particles smaller than 0.1 mm are transported in suspension over longer distances and eventually deposited as loess (Fig (I - 6)), particles larger than 0.3 mm move mainly by rolling and tend to concentrate in the residual sand layer. Although aeolian sediments composed of mixtures of these sizes are found in some transitional environments, wind action is relatively efficient in separating the coarse, medium, and silt fractions. Perfect separation of particles of different sizes does not occur because aeolian sand transport is a stochastic process in which the trajectories of individual particles are affected to varying degrees by random turbulent fluctuations in the wind as well as considerable natural variability. Cereals bed collision [Ungar & Haff 1987, Anderson 1987a]. [Pye, Kenneth, and Haim Tsoar, (2008)].

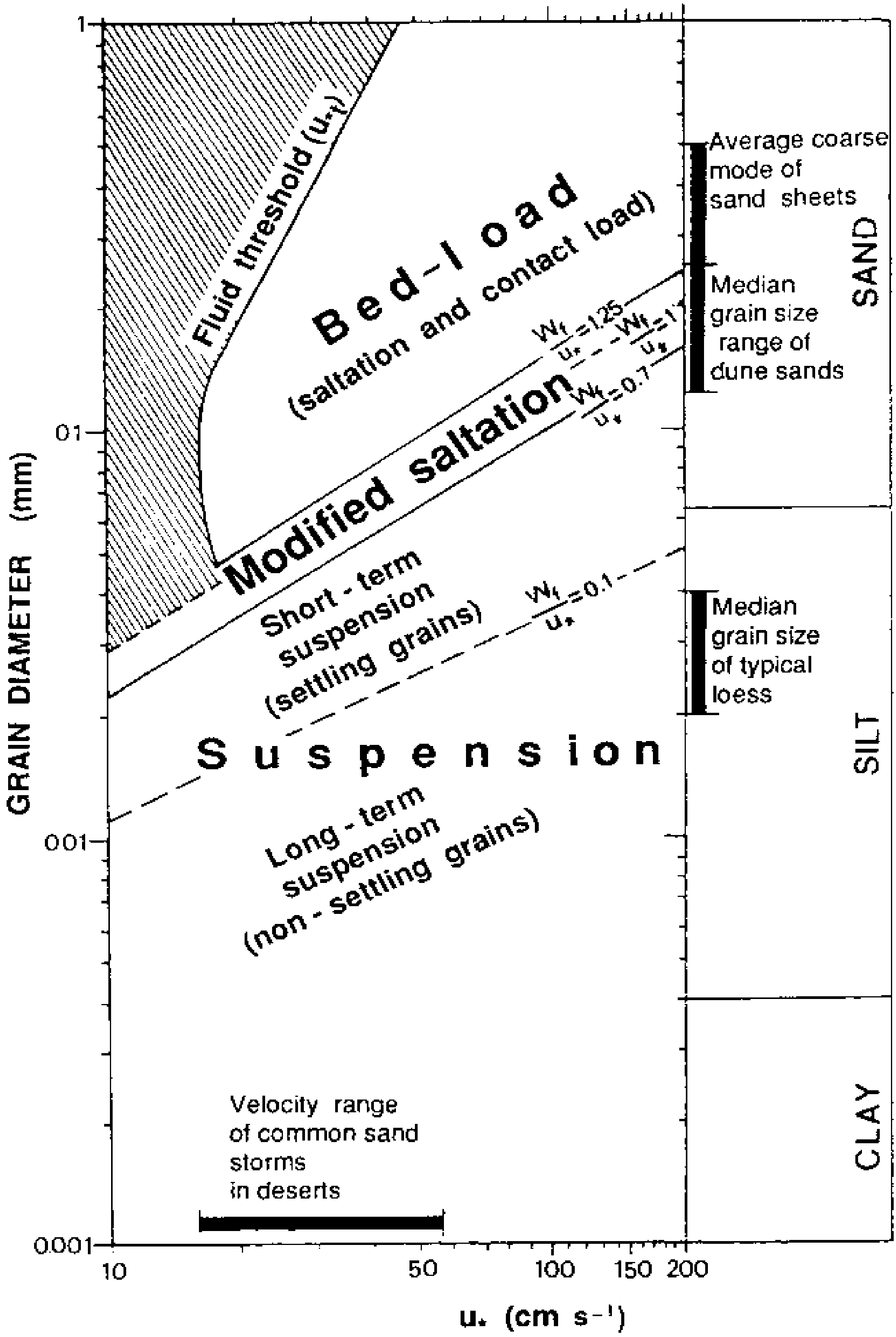

Figure (I - 6): Mods of transport of quartz spheres at different wind shear velocities.

(After Tsoar & Pye 1987)

I.3.2 Suspension

Suspended transport occurs when the vertical velocity change associated with air turbulence is greater than the particle settling velocity, as described above. The sinking velocity of quartz spheres in the size range 0.001-0.05 mm can be determined using Stokes' law [Green & Lane 1964, p. 67]: $w_f = Kd^2$ where d is the diameter and K is $\rho_s g/18\,\mu$(where ρ_s the grain density, g is the acceleration of gravity, and μ is the dynamic viscosity of air). For a quartz sphere, K in air at sea level is taken as 8.1×105$cm^{-1}s^{-1}$. In a typical sandstorm, when the value of u^* ranges from 0.18 and 0.6ms^{-1}, the maximum particle size range that can be transported by the corresponding suspended particles is 0.04 to 0.06 mm in diameter (Fig (I - 6)).

In order to remain suspended in the atmosphere for a considerable period of time, particles must experience a high ratio of upward to downward movements.

When $w_f/u^* = 0.4$, the ratio is 0.5, and there is little chance that the grain will be suspended for a long time. Long-term suspension requires a w_f/u^* ratio of < 0.1, which corresponds to a maximum particle size of 0.015–0.02 mm in typical storms (Fig (I - 6)). [Gillette 1979, 1981] Particles smaller than this size are called non-settling particles, while larger silt particles are called settled particles. Typical loess sediments are mainly composed of settled particles transported by short-term suspension, while the particles transported over long distances in the ocean are mainly composed of non-settled particles transported by long-term suspension. [Tsoar & Pye 1987, Pye 1987]. [Pye, Kenneth, and Haim Tsoar, (2008)].

I.3.3 Saltation

The word jump (from the Latin saltare = to jump) was first introduced by McGee (1908) to describe the jumping motion of grain carried by running water along a riverbed. Joly (1904) and Owens (1927) were among the first to describe this phenomenon in wind energy transport. Bagnold (1936) and subsequently Chepil (1945a) and Zingg (1953b) photographically demonstrated the characteristic ballistic trajectories of salt particles in air (Fig (I - 7)).

The nature of jumps has been extensively studied by a series of wind tunnels, numerical simulations, and field methods [Bagnold 1936, 1941, Owen 1964, 1980].

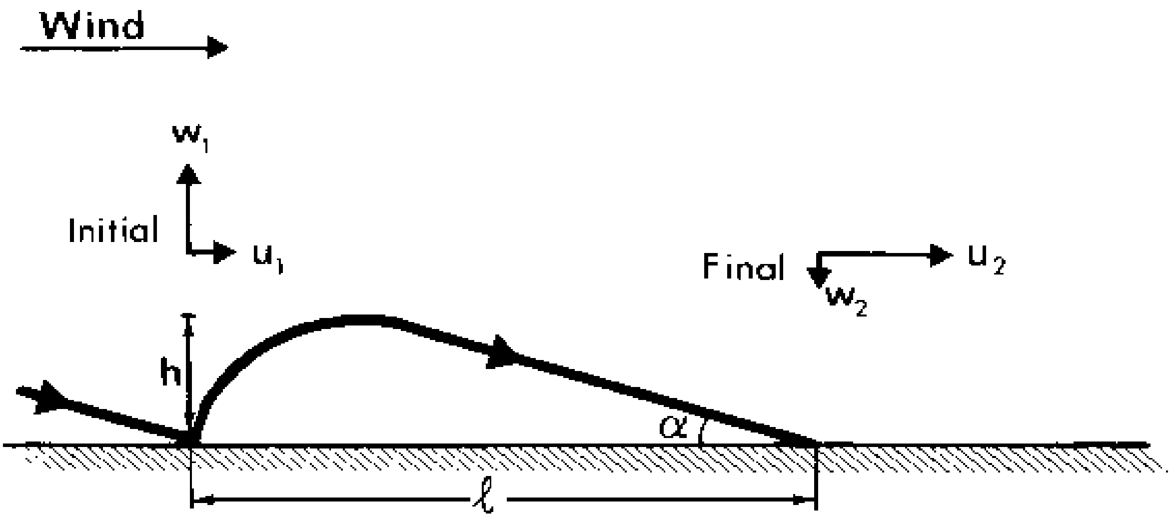

Figure (I - 7): Characteristic path of a saltating grain; h and ℓ are the maximum jump height and jump lengths, respectively, α is the impact angle, $w_1$and w_2 are the initial and final vertical velocities, and $u_1$and $u_2$are the initial and final horizontal velocities of the grain. (After Bagnold 1937b).

These studies show that the type and rate of salt formation is influenced by a variety of factors, including particle size and shape, wind speed (represented byu^*), and the surface properties of salt formation.

Due to the large density difference between air and transported quartz particles (ρ_S/ρ= 2150), the sedimentation rate of quartz particles in air is 60–80 times higher than in water. Particles transported in air require 29 times the fluid velocity required to transport particles of the same size in water. Furthermore, the impact force of grain in air is much greater than that of grain transported in water [Iversen et al. 1987]. Therefore, in water very few particles are removed from the bed due to the influence of saline particles, which is the main mechanism for particle movement during Aeolian sand transport.

The effectiveness of salinization in the air reflects the occurrence of a positive feedback process in which some of the grains initially swept by aerodynamic drag create a chain reaction where each impacted grain causes several others to be lifted from the bed squirting. However, the presence of salt particles changes the wind speed profile near the ground, making it a self-regulating mechanism.

The trajectories of the salt grains in the air depend on whether the grain is entrained by direct fluid buoyancy/drag or other salt grain effects, or whether the grain has become salted and left the bed in a series of jumps called sequential jumps [Tsuchiya 1970] Many grains have been observed to rise almost vertically from the bed, but recent studies have reported an average rise angle of between 34° and 50° relative to the horizontal [Tsuchiya 1970, N].

Grain that bounced off the surface during salting had a lower average rise angle (21-33°, higher values were for coarser grains) than grains that "splashed" out of the bed on impact (52-54°; [Wilitz and Rice 1985a]). This can be explained in part by the large amount of forward momentum that the bouncing particles have on impact, and in part by the slower ascent of the ejected particles and therefore longer residence times near the most buoyant bed [Anderson and Hallett 1986]. On the other hand, horizontal resistance increases with height [Chepil 1961]. (Fig (I - 8)) shows in two dimensions the pressure distribution pattern and the resultant force exerted on the surface of an 8 mm diameter sphere subjected to a friction velocity of 98 cms^{-1}. It was found that lift vanished at an altitude of approximately 2.5 cm, while drag continued to increase with altitude in proportion to wind speed. Additional lift can be created as particles rotate as they move along their trajectories. Bagnold (1936) reported little grain rotation, but Chepil (1945a) observed that about 75% of the grains were rotated at 200-1000 r.p.s. White & Schulz (1977), who estimated the spin rate to be 115-500 r.p.s. Revolutions per second, also emphasized particle spin. White (1982) reported an average particle spin rate of 350-400 r.p.s. Revolutions per second. As the grain rotates, the airflow lines around the grain become asymmetrical. At the bottom of the grain (point Q in Figure (I- 10)), the air in and around the grain moves against the wind. At the top (point P in Figure (I- 10)), they move in the same direction as the wind current. According to Bernoulli's equation: $p_t = p_s + \frac{1}{2}\rho U^2 = constant$ Where p_t is the total pressure, also known as dynamic pressure because it also exists when the flowing air is at rest. The term $p_s$stands for static pressure; this is the pressure felt on a surface on which air is flowing. It is easy to measure without disturbing the flow, such as through holes in the surface. The term$\frac{1}{2}\rho U^2$, known as the dynamic pressure of the flow, is an expression of the kinetic energy of the flow. This creates a pressure difference between P and Q (and between R and S). The buoyancy is perpendicular to the flow direction and the particle's axis of rotation. This type of buoyancy, known as the magnus effect, is important for sand particles larger than 0.1 mm in diameter [White & Schulz 1977]. The bouncing grain begins to spin after hitting the surface with a swipe .The rotational speed is maximum immediately after impact and decreases as the particle progresses along its trajectory. A comparison of the observed and calculated theoretical

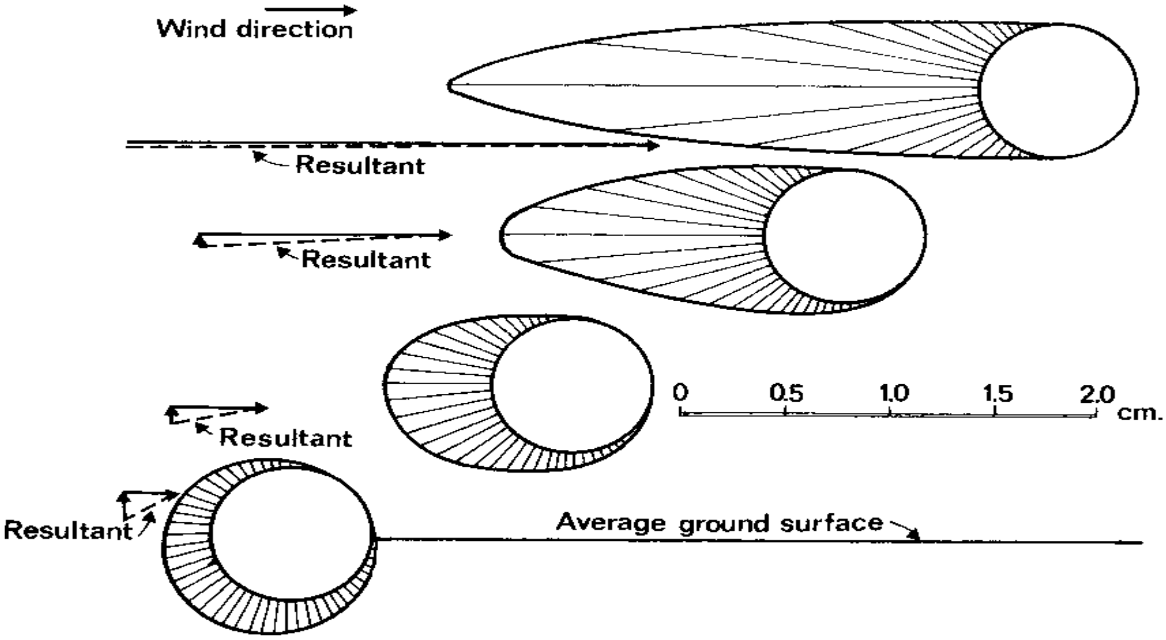

Figure (I - 8): Pattern of pressure around a sphere, 8mm in diameter, subjected to a friction velocity of 98 cms^{-1}at various heights above the ground. Also shown is the resultant force acting on the grain at different heights. (After Chepil 1961)

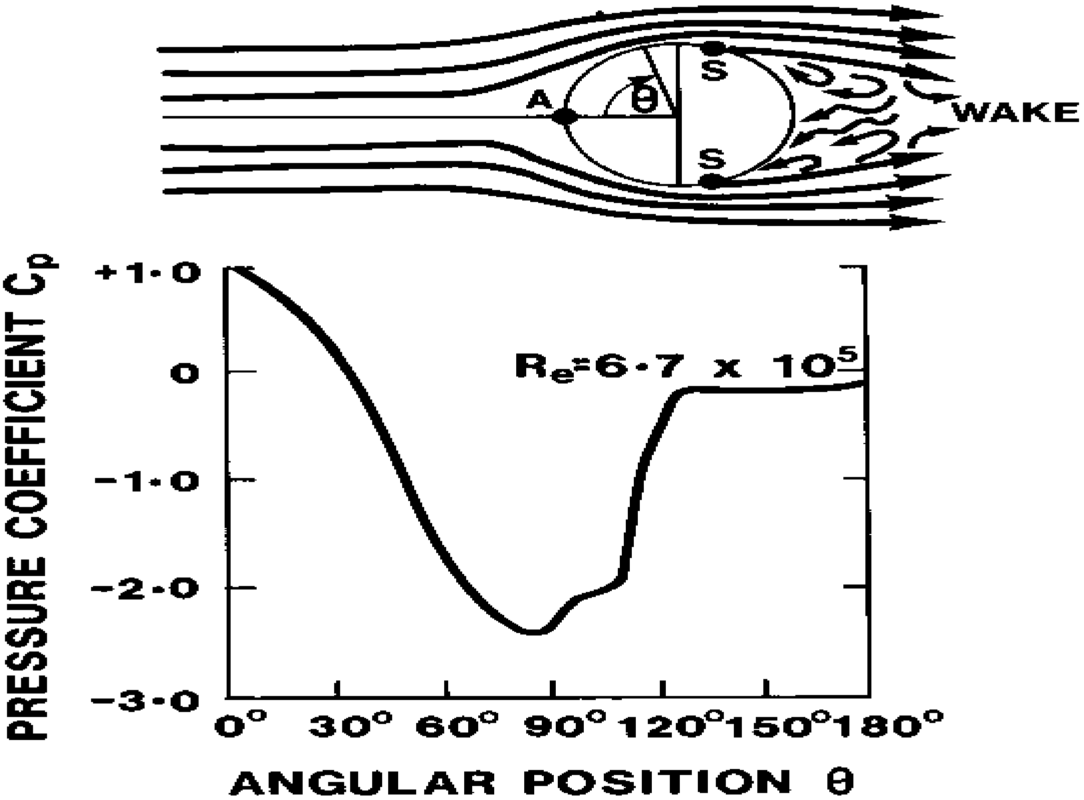

Figure (I - 9): Pressure distribution around a cylinder. A indicates the stagnation point and S the separation points. (Adapted from Mironer 1979, reproduced by permission of McGraw–Hill)

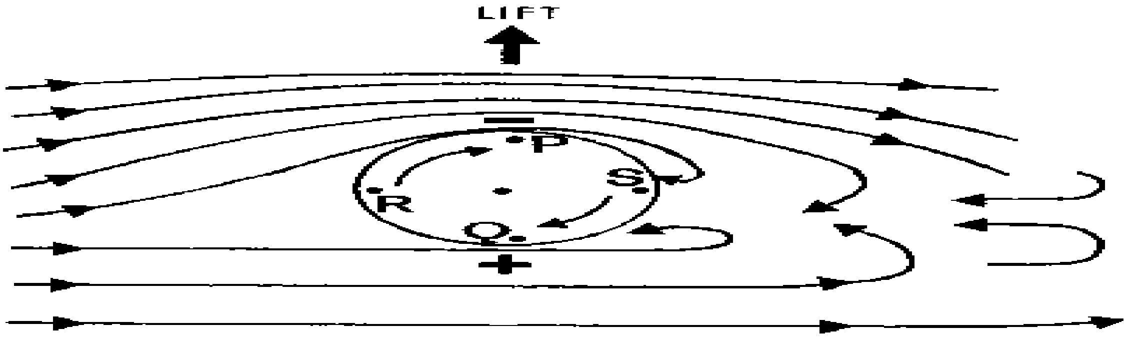

Figure (I - 10): Effect of grain spin in producing additional lift (Magnus effect). In addition to streamline asymmetry and the resulting pressure difference on the front and back of the grain (**cf**. Figure (I-9)**)**, there is also asymmetry above and below the grain. Velocity is high near P, where the airflow is reinforced by the spinning motion of the grain, and low near Q, where the grain's rotation opposes the airflow.

trajectories shows good agreement when considering the magnus effect corresponding to rotation rates of 100–500 r.p.s. [Weiss and Schultz 1977, Weiss 1982]. However, Jensen & Sørensen (1983) and Hunt & Nalpanis (1985) challenge these results. These two forces cancel the buoyant force exerted on the particle: resistance $F_d = C_D \frac{1}{2} \rho U^2 A$. Where A is the largest projection area of the body and the product $\frac{1}{2} \rho U^2$ is the dynamic pressure. C_D is a dimensionless drag coefficient that depends on a number of factors, the most important being the shape of the body, but also including the reynolds number and surface roughness. The shape and projected area of the particles or bed forms exposed to the wind are the factors which principally determine the drag and the downward force of the grain's own weight $W = C_S \rho_s' \, gd^3$. Where $\rho_s'$is the density of the immersed grain (ρ_s'=ρ_s−ρ, $\rho_s$being the grain density and ρ the fluid density) and $C_S$is a shape coefficient such that $C_S d^3$ is the volume of the grain (for a sphere C_S= 0.524).Experiments have shown that during .Because the density of air is much less than that of water, the gravity in the air is more obvious. In the case of a 1 mm diameter spherical particle lifted with a vertical velocity (w_1) of 10cms^{-1}, Gravity is approximately 1300 times the drag [Middleton & Southard 1978]. In the absence of drag and buoyancy, if all kinetic energy could be converted into potential energy, the bouncing particle would rise to a height of $w_1^2/2g$. However, the maximum rise during the jump is less than $w_1^2/2g$, which depends on grain size; grain advance speed and rise angle [Anderson & Hallet 1986]. The smaller the grain, the greater the resistance effect, the lower the climb rate, and the greater the horizontal acceleration. If w_1=70cm$s^{-1}$and u^* =20cms^{-1}, 0.2mm diameter beads have a maximum rate of rise of $0.7\, w_1^2/2g$, but 0.1mm diameter beads increase at a maximum rate of$0.53 w_2^2/2g$ [Nalpanis 1985]. Relationship between mean rise

(h), friction velocity (u^*) and particle size (d) for several well- classified grit size ranges, Zingg (1953a) found that

$$h = 0.782 d^{\frac{3}{2}} u^{*\frac{1}{2}} \qquad \text{(I - 1)}$$

Where h is in cm, d is in mm, and u^* is in cms^{-1}, (Figure (I- 11)). Observations during moderate-intensity dust storms also confirm that larger particles bounce off more easily than smaller particles [Chepil & Milne 1939, Bagnold 1960, Sharp 1964].

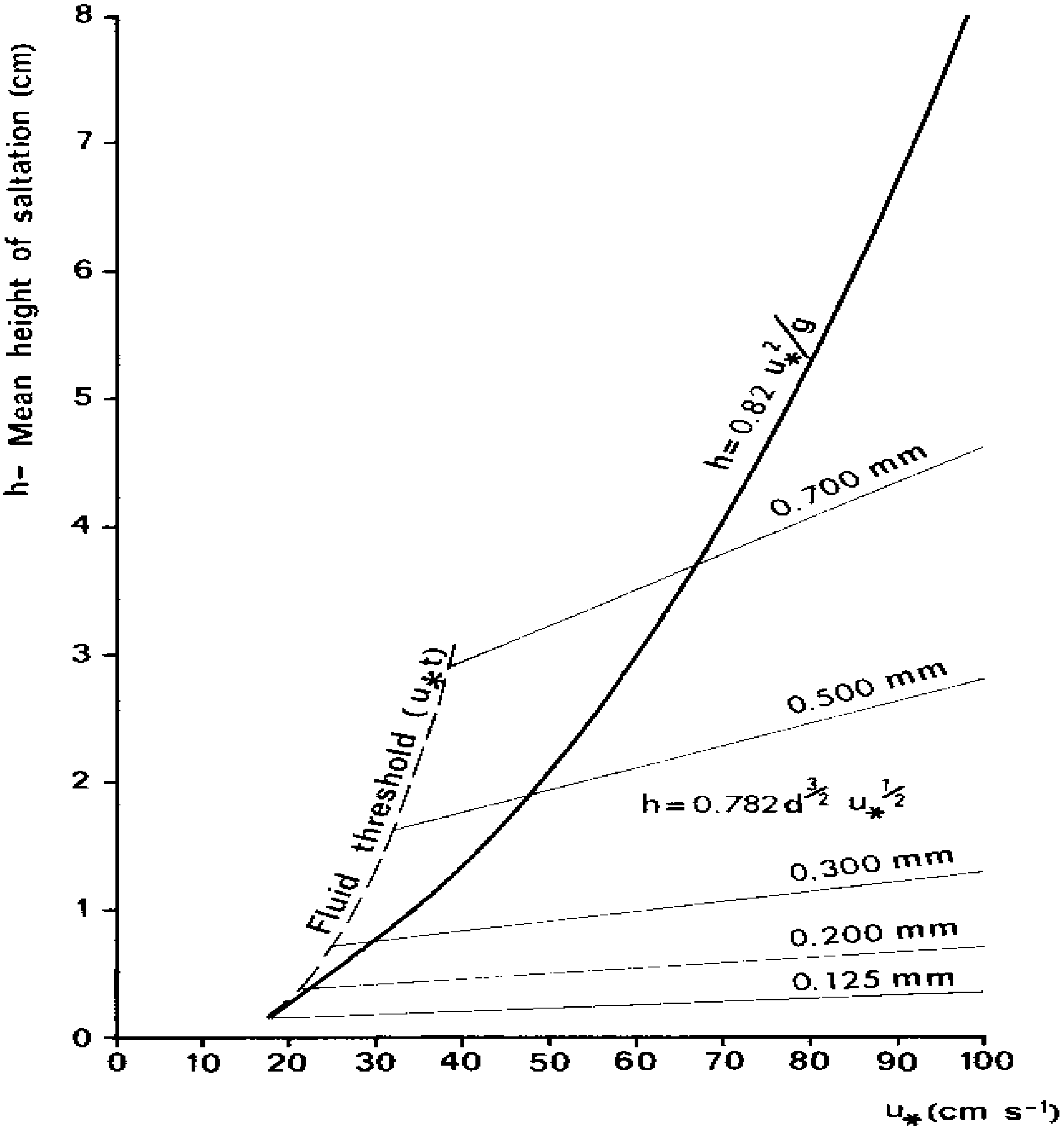

Figure (I - 11): Mean ascent height of saltating sand as a function of friction velocity (bold line), according to Owen's (1980) theoretical analysis, and as a function of grain size and friction velocity for uniform sand (**thin lines**), according to the empirical analysis of Zingg (1953a)

Wind tunnel studies have shown that the average size of salt grains generally decreases with height above the surface, reaching at least 2 cm in height [Gerety & Slingerland 1983, Williams 1964]. Particle size at any given height will increase with u^*, since coarse particles tend to bounce higher in strong winds. However, most of the particles near the top of the salt layer were small, probably because the small particles were lifted to higher heights by the turbulent eddies (ie, these particles were transported in the modified saline). In field studies, De Ploey (1980) and Draga (1983) observed a reduction in size

The height of the salt grains, although a large number of coarse grains have been found to bounce more than 50 cm above the surface. The salt layer has no well-defined upper limit, but its maximum height is about 10 times the average salt layer height (usually less than 1 cm in wind tunnel studies). Field measurements of clay particles in brackish water with wind velocities of 7-10 ms^{-1} measured at a height of 30 cm resulted in an average brackish water height of about 5 cm [Chepil & Milne 1939]. Particles of various sizes bounce higher on hard desert surfaces such as stone pavements and gravel fans than on loose sand [Bagnold 1941, p. 36, Sharp 1964] (Figure (I-12)). The maximum salt depth of such hard surfaces can exceed 3 m, and the average salt depth is more than 20 cm. The distribution of particle flow with height during salinization is highly skewed, with the highest particle concentrations found near the bed. According to Owen's (1980) theoretical calculation, the average jump height is 0.82 u*2/g, and the average jump path length is 10.3 u*2/g (Figure (I-13)). Owen predicts that the average horizontal distance during a jump is about 12 times the average maximum jump height. This ratio is higher than that measured by Bagnold (1936) and Chepil (1945a) and calculated by Tsuchiya (1970), but lower than that predicted by White & Schulz (1977). The height and length of the jump path depend on particle shape, particle size and friction velocity. [Williams (1964) and Willetts (1983)].

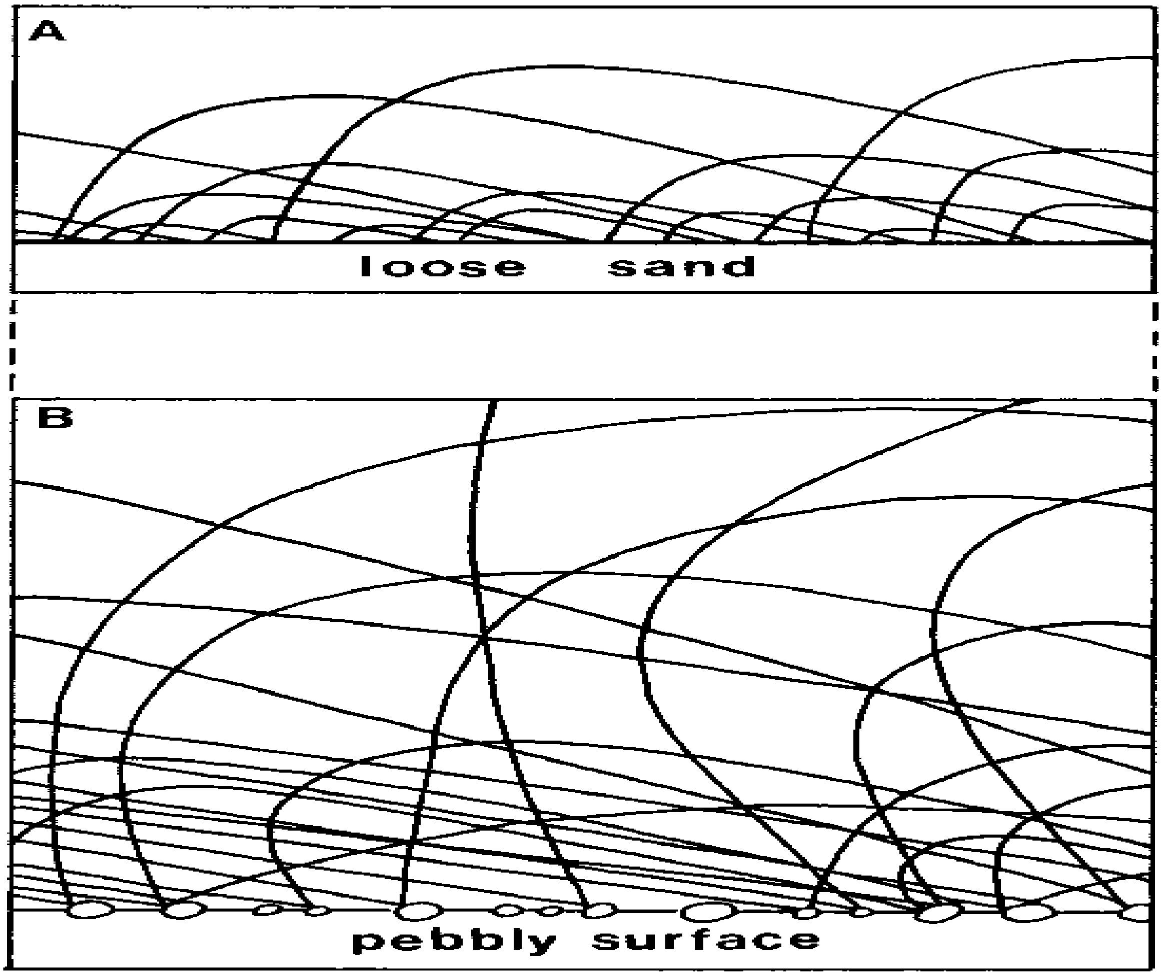

Figure (I - 12): Schematic representation of saltation trajectories over (**A**) a loose sand and (**B**) a pebbly surface.

(After Bagnold 1941, p. 36).

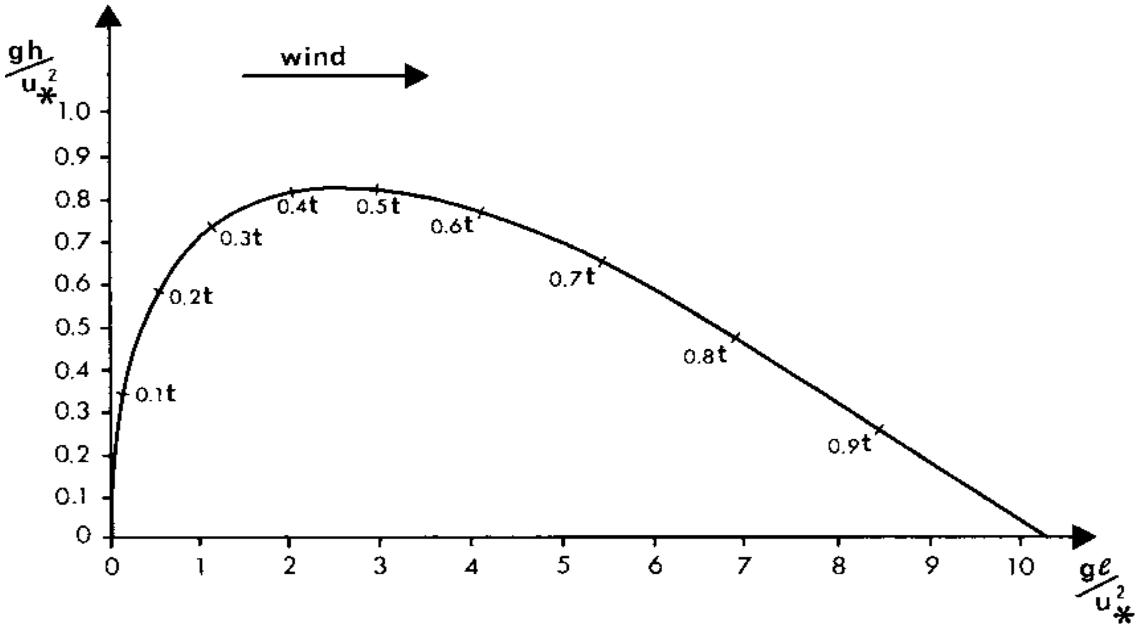

Figure (I - 13): Depiction of the mean saltation trajectory after Owen; (h) is the maximum jump height, l is the horizontal distance between the lift-off point and the impact point, and (t) is the time taken to complete the trajectory. The coordinates are non-dimensional and the ordinate scale is exaggerated by a factor of five.

It has been observed that low spherical particles move on flatter, longer trajectories compared to spherical particles. The flight time of a particle from start to landing is about 0.1-0.2 s [Anderson & Hallet 1986]. It takes about half the time for a particle to reach the vertex of its trajectory. The initial ascent rate (w_1) of the characteristic particles is proportional to the friction rate, since the characteristic particles are assumed to be ejected from the surface by the average force of the impinging particles whose terminal velocity is controlled by u^* [Bagnold 1936 , 1937b, Owen 1964]. Thus w_1 = Bu^*, where B, the collision coefficient, was found to be 0.8 for a typical grain size of 0.25 mm [Bagnold 1936]. Recent studies have shown higher values for the shock coefficient, around 2 [White & Schulz 1977, Nalpanis 1985].

After reaching the apex, the grain begins to fall at an increasing rate. Calculations by Hunt & Nalpanis (1985) show that the horizontal velocity of sand grains (approximately 0.2 mm in diameter) at the apex of the trajectory is about half the average wind velocity at the same height. As the grain sinks, the resistance of the wind causes horizontal acceleration. Since the average resistance is greater than gravity, the grain hits the surface at an angle of 6-20° (14° on average). This angle decreases with decreasing grain size [Bagnold 1936, Chepil 1961]. As the impact angle decreases, the energy consumed by the impact bed decreases, and the impact particles bounce back, retaining most of the energy. Willetts & Rice (1985a) found that the mean ascent velocity (0.15–0.25 mm) of rebound fine sand was 240 cms^{-1}. (Approximately 3 to 5 times its ascent velocity), while the mean ascent rate of the same size only 31 cms^{-1}.

Because they are accelerated by the wind, the grains fall with more energy than when they leave the surface. Particles leaving the surface strike the surface with 3 to 5 times the initial velocity or 10 to 20 times the initial kinetic energy at different vertical velocities [Anderson & Hallet 1986]. A portion of this energy is dissipated by inelastic deformation and frictional rotation of the particles in the bed. During this burst, several new particles can be ejected into the flow. Sometimes the impacted grain will burrow into the bed, but more often it will bounce off the surface with variable energy loss. [Mitha et al. (1986)] observed that when a rebound occurs, several other particles are usually ejected at low energies from an area centred on about ten particle sizes directly in front of the impact point. Up to ten particles can be ejected per impact, and the average ejection velocity of each particle is less than 10% of the impact velocity [Willetts & Rice 1986a].

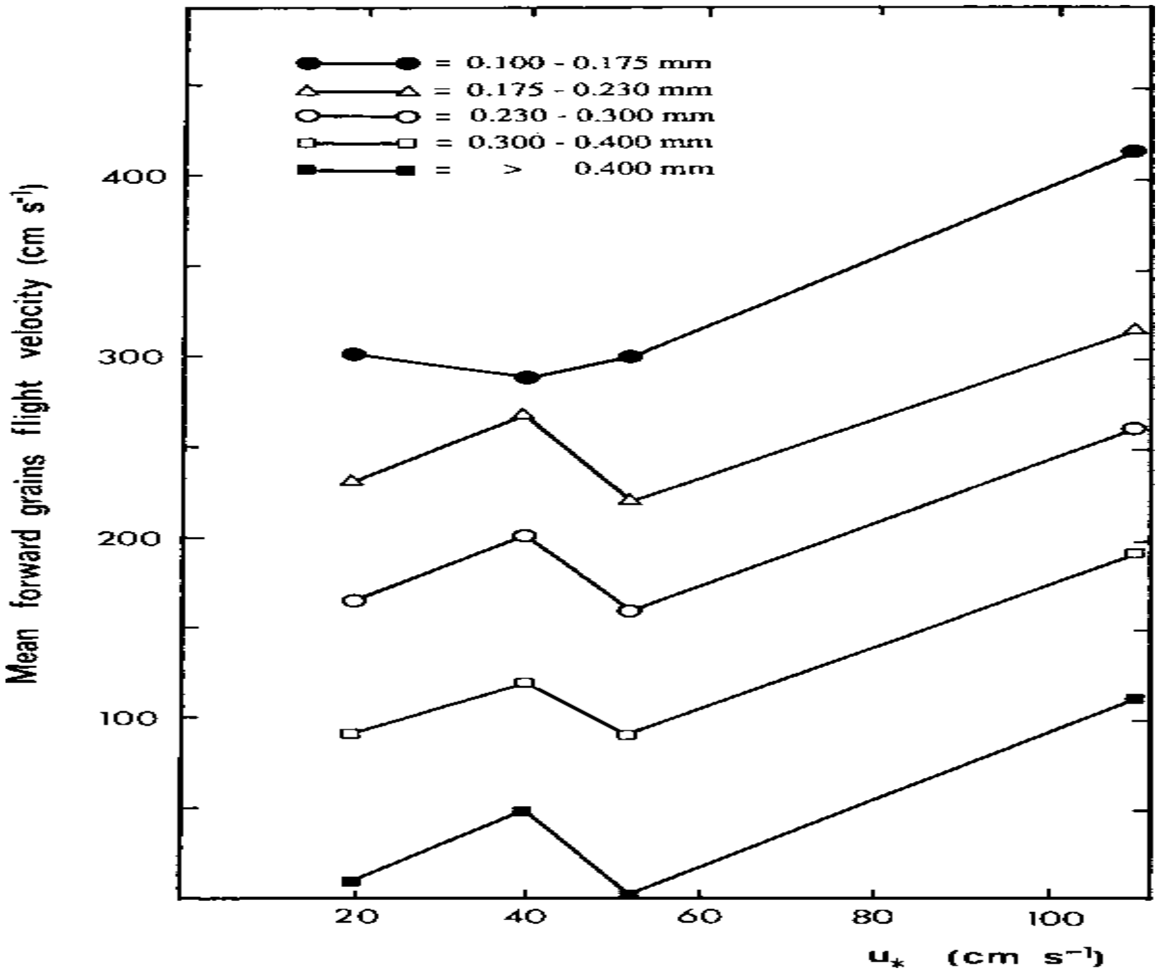

Figure (I - 14): Variation in estimated mean forward grain velocities with $u^*$for different sizes of quartz grains.

(Data of Gerety 1984)

The salt particles extract momentum from the wind, modify the wind velocity profile near the bottom, and reduce the friction velocity below the fluid threshold. The transport of sand grains is then maintained entirely by the action of salt grains [Bagnold 1973, Anderson 1987b]. Eventually, an equilibrium state called the steady-state transition is reached between the near-surface wind speed and the particles in the transition. Even if the average wind speed is constant, individual grains do not jump continuously. After a few bounces, a grain of salt can come to rest before being mobilized again by the shock of another. Wind tunnel experiments show that the average forward motion speed decreases proportionally with increasing grain size. In laboratory, wind tunnel experiments [Barndorff-Nielsen et al. (1985b)] found that sand grains in the size range 0.28-0.48 mm had an average forward velocity of 0.6-1.8 cms^{-1}, including stationary periods but excluding time buried under waves. As the friction velocity increases, the average forward velocity increases, although not by much (Figure (I-14)) [White & Schulz 1977]. [Pye, Kenneth, and Haim Tsoar, (2008)].

Chapter II : Mathematical Modelling

II.1 Introduction

The model to the Euler-Euler model is based on averaging the Navier-Stokes equations for each phase over a volume that is small compared to the computational domain but large compared to the dispersed phase (particles, droplets, or bubbles). . The physics model solves a set of momentum equations for each phase, assuming that the continuous and dispersed phases behave as two continuous and interpenetrating fluids. [CFD Module User's Guide COMSOL].

II.2 Euler Euler turbulent flow model

The Euler-Euler model, the turbulent flow model, located under the multiphase flow branch of the Euler-Euler model when a physical model is added, can be used to simulate the flow of a high Reynolds number for a two-phase mixture containing a continuous and a dispersed phase. The Euler Euler model assumes that both phases are continuous, completely overlapping, and incompressible. Typical applications of the model are fluidized layers (solid particles in a gas), sedimentation (solid particles in a liquid), or the transfer of liquid droplets or bubbles in a liquid.

The physics model solves two sets of Navier-Stokes equations, one for each phase, in order to calculate the velocity field for each phase. Momentum exchange phases as shown in the drag model. The pressure is calculated from the mixture mean continuity equation and the volume fraction of the dispersed phase is traced using the transfer equation.

The two-stage perturbation is modelled using the k-ε standard two-equation model with probe constraints. The model includes the possibility to solve one set of k-ε equations for a two-phase mixture, or to solve two sets of k- ε equations, one for each phase. The flow is designed near the walls using wall posts. [CFD Module User's Guide COMSOL].

II.2.1 Turbulence

Turbulence Model Type: The default Turbulence model type is RANS, *k*-*ε*. [CFD Module User's Guide COMSOL].

- **RANS(*k*-*ε*):**

There are numerous RANS models, but in this work, we will consider only the standard *k*-*ε* model (which is perhaps the most widely used RANS model). The Reynolds-averaged equations for continuity and momentum for steady, incompressible flow are as follows:

$$\frac{\partial U_i}{\partial x_i} = 0 \qquad \text{(II – 1)}$$

And

$$\frac{\partial (U_i U_i)}{\partial x_i} = -\frac{1}{\rho}\frac{\partial p}{\partial x_i} + \frac{\partial}{\partial x_j}\left(\nu \frac{\partial U_i}{\partial x_j} - \overline{u_i' u_i'}\right) \qquad \text{(II – 2)}$$

Here, U_i and $u_i'$are the mean and fluctuating velocities in the x_i-direction, respectively, and p is the mean pressure. The presence of the Reynolds stresses $\overline{u_i' u_i'}$; in Equation (II – 2) implies that the latter are not closed. The Reynolds averaging of a quantity is denoted by drawing a bar over that quantity. Closure requires that some approximations be made in prescribing the Reynolds stresses in terms of the mean flow quantities. The most popular statistical turbulence closure model is the Boussinesq type of eddy viscosity approximation that assumes a linear relationship between the turbulent stresses and the mean velocity gradients:

$$-\overline{u'_i u'_i} = \nu_t^* \left(\frac{\partial U_i}{\partial x_j} + \frac{\partial U_i}{\partial x_i}\right) - \frac{2}{3} k \delta_{ii} \qquad \text{(II – 3)}$$

Where ν_t^* is the kinematic eddy viscosity and $k \equiv \frac{1}{2}\overline{u_i' u_i'}$ is the turbulence kinetic energy (TKE). In the standard *k*-*ε* model, ν_t^* is determined as

$$\nu_t^* = C_\mu \frac{k^2}{\varepsilon} \qquad \text{(II – 4)}$$

Where ε is the dissipation of TKE. The standard model uses the following transport equations for *k* and *ε*:

$$\frac{\partial (U_i k)}{\partial x_j} = \frac{\partial}{\partial x_j}\left[\left(\nu + \frac{\nu_t^*}{\sigma_k}\right)\frac{\partial (k)}{\partial x_j}\right] + \nu_t^* \left(\frac{\partial U_i}{\partial x_j} + \frac{\partial U_i}{\partial x_i}\right)\frac{\partial U_i}{\partial x_i} - \varepsilon \qquad \text{(II – 5)}$$

And

$$\frac{\partial (U_i \varepsilon)}{\partial x_j} = \frac{\partial}{\partial x_j}\left[\left(\nu + \frac{\nu_t^*}{\sigma_\varepsilon}\right)\frac{\partial (\varepsilon)}{\partial x_j}\right] + C_{\varepsilon 1}\frac{\varepsilon}{k}\, \nu_t^* \left(\frac{\partial U_i}{\partial x_j} + \frac{\partial U_i}{\partial x_i}\right)\frac{\partial U_i}{\partial x_i} - C_{\varepsilon 2}\frac{\varepsilon^2}{k}\, \varepsilon \qquad \text{(II – 6)}$$

The equations contain five closure constants: namely, C_μ , σ_k , σ_ε , $C_{\varepsilon 1}$, and $C_{\varepsilon 2}$.The standard k-ε model employs values for constants that are determined by a comprehensive data fitting over a wide range of canonical turbulent flows. See in Table ((II - 1)).

The turbulent diffusion of k and ε in Equation (II – 5) and (II – 6), respectively, are represented using a gradient diffusion hypothesis with the Prandtl numbers σ_k and σ_ε used to connect the eddy diffusivities of k and ε to the eddy viscosity ν_t^*. [Cheng, Y., Lien, F. S., Yee, E., & Sinclair, R. (2003)].

- **Two-phase turbulence:**

The Two-Phase Turbulence is defined as Mixture. This implies that one set of k-ε equations are solved for. To instead solve for two sets of k-ε equations, one for each fluid phase, select Phase specific (see Turbulent Two-Phase Flow Modelling). [CFD Module User's Guide COMSOL].

II.2.2 The Euler-Euler Model Equations

a) Mass Balance

Assuming that the mass transfer between the two phases is zero, the following continuity relations hold for the continuous and dispersed phases [C. Crowe, M. Sommerfeld, and Y Tsuji, 1998]:

$$\frac{\partial}{\partial t}(\rho_c\, \phi_c) + \nabla . (\rho_c\, \phi_c\, u_c) = 0 \qquad \text{(II – 7)}$$

$$\frac{\partial}{\partial t}(\rho_d\, \phi_d) + \nabla . (\rho_d\, \phi_d\, u_d) = 0 \qquad \text{(II – 8)}$$

Here ϕ (dimensionless) denotes the phase volume fraction, ρ (kg/m^3) is the density, and u (m/s) the velocity of each phase. The subscripts c and d denote quantities relating to the continuous and the dispersed and phase, respectively. The following relation between the volume fractions must hold

$$\phi_c = 1 - \phi_d$$

Both phases are considered to be incompressible, in which case Equation (II – 7) and Equation (II – 8) can be simplified as:

$$\frac{\partial \phi_c}{\partial t} + \nabla . (\phi_c\, u_c) = 0 \qquad \text{(II – 9)}$$

$$\frac{\partial \phi_d}{\partial t} + \nabla . (\phi_d\, u_d) = 0 \qquad \text{(II – 10)}$$

If Equation (II – 9) and Equation (II – 10) are added together, a continuity equation for the mixture is obtained:

$$\nabla . \big((\phi_d\, u_d) + u_c(1 - \phi_d)\big) = 0 \qquad \text{(II – 11)}$$

In order to control the mass balance of the two phases, the Euler-Euler Model solve Equation (II – 9) together with Equation (II – 11). Equation (II – 9) is used to compute the volume fraction of the dispersed phase, and Equation (II – 11) is used to compute the mixture pressure. [CFD Module User's Guide COMSOL].

b) Momentum Balance

The momentum equations for the continuous and dispersed phases, using the non-conservative forms of Ishii [B.G.M. van Wachem, J.C. Schouten, C.M. van den Bleek, R. Krishna, and J.L. Sinclair, 2001] are:

$$\rho_c\, \phi_c \left[\frac{\partial}{\partial t}(u_c) + u_c \nabla . (u_c)\right] = -\phi_c \nabla p + \nabla . (\phi_c\, \tau_c) + \phi_c\, \rho_c g + F_{m,c} + \phi_c\, F_c \qquad \text{(II – 12)}$$

$$\rho_d \phi_d \left[\frac{\partial}{\partial t}(u_d) + u_d \nabla . (u_d)\right] = -\phi_d \nabla p + \nabla . (\phi_d\, \tau_d) + \phi_d\, \rho_d g + F_{m,d} + \phi_d\, F_d \qquad \text{(II –13)}$$

Here p (Pa) is the mixture pressure, which is assumed to be equal for the two phases. In the momentum equations the viscous stress tensor for each phase is denoted by τ (Pa), g (m/s^2) is the vector of gravitational acceleration, F_m(N/m^3) is the interphase momentum transfer term (that is, the volume force exerted on each phase by the other phase), and F **(**N/m^3) is any other volume force term.

For fluid-solid mixtures, Equation (II – 13) is modified in the manner of [H. Enwald, E. Peirano, and A.-E. Almstedt, 1996]

$$\rho_d\ \phi_d \left[\frac{\partial}{\partial t}(u_d) + u_d \nabla\,.(u_d)\right] =$$

$$-\phi_d \nabla p + \nabla\,.(\ \phi_d\ \tau_d) - \nabla p_s + \phi_d\ \rho_d g + F_{m,d} + \phi_d\ F_d \qquad \text{(II – 14)}$$

Where p_s (Pa) is the solid pressure.

The fluid phases in the above equations are assumed Newtonian and the viscous stress tensors are defined as

$$\tau_c{=}\mu_c \left(\nabla u_c + (\nabla u_c)^T - \tfrac{2}{3}(\nabla.u_c)I\right)$$

$$\tau_d{=}\mu_d \left(\nabla u_d + (\nabla u_d)^T - \tfrac{2}{3}(\nabla.u_d)I\right)$$

Where μ (Pa·s) is the dynamic viscosity of the respective phase.

In order to avoid singular solutions when the volume fractions tend to zero, the governing equations above are divided by the corresponding volume fraction. The implemented momentum equation for the continuous phase is:

$$\rho_c \frac{\partial}{\partial t}(u_c) + p_c u_c \nabla.(u_c) = -\nabla p + \nabla\,.\tau_c + \frac{\nabla \phi_c.\tau_c}{\phi_c} + \rho_c g + \frac{F_{m,c}}{\phi_c} + F_c$$

The implemented momentum equation for the dispersed phase in the case of dispersed liquid droplets or bubbles is:

$$\rho_d \frac{\partial}{\partial t}(u_d) + p_d u_d \nabla.(u_d) = -\nabla p + \nabla\,.\tau_d + \frac{\nabla \phi_d.\tau_d}{\phi_d} + \rho_d g + \frac{F_{m,d}}{\phi_d} + F_d \qquad \text{(II –15)}$$

And in the case of dispersed solid particles:

$$\rho_d\ \frac{\partial}{\partial t}(u_d) + p_d u_d \nabla.(u_d)$$

$$-\nabla p + \nabla\,.\tau_d + \frac{\nabla \phi_d.\tau_d}{\phi_d} - \frac{\nabla p_s}{\phi_d} + p_d g + \frac{F_{m,d}}{\phi_d} + F_d \qquad \text{(II – 16)}$$

II.2.3 Dispersed Phase Viscosity

The Newtonian viscosities of interpenetrating media are not readily available. Instead, various researchers have developed empirical and analytical models for the dynamic viscosity of the two-phase mixture, usually as a function of the dispersed volume fraction. Using an expression for the mixture viscosity.

The default values for the dynamic viscosities of the two interpenetrating phases are taken to be:

$$\mu_C = \mu_D = \mu_{mix} \qquad \text{(II – 17)}$$

A simple mixture viscosity covering the entire range of particle concentrations is the Krieger type model [H. Enwald, E. Peirano, and A.-E. Almstedt, 1996]:

$$\mu_{mix} = \mu_c \left(1 - \frac{\phi_d}{\phi_{d,max}}\right)^{-2.5\phi_{d,max}} \qquad \text{(II – 18)}$$

Here $\phi_{d,max}$ is the maximum packing limit, by default 0.62 for solid particles. Equation (II – 18) can be applied when $\mu_c \ll \mu_d$. An extension of Equation (II – 18)

Can be applied for liquid droplets/bubbles:

$$\mu_{mix} = \mu_c \left(1 - \frac{\phi_d}{\phi_{d,max}}\right)^{-2.5\phi_{d,max}\frac{\mu_d + 0.4\mu_c}{\mu_d + \mu_c}} \qquad \text{(II – 19)}$$

For liquid droplets/bubbles the default value of $\phi_{d,max}$ is 1.

II.2.4 Inter Phase Momentum Transfer

In all the equations, F_m denotes the interphase momentum transfer that is the force imposed on one phase by the other phase. Considering a particle, droplet, or bubble in a fluid flow, it is affected by a number of forces, for example, the drag force, the added mass force, the Basset force, and the lift force. The most important force is usually the drag force, especially in fluids with a high concentration of dispersed solids, and hence this is the predefined force included in the Euler-Euler model. The drag force added to the momentum equation is defined as:

$$F_{drag,c} = -F_{drag,d} = \beta \boldsymbol{u_{slip}} \qquad \text{(II – 20)}$$

Where β is a drag force coefficient and the slip velocity is defined as [CFD Module User's Guide COMSOL].

$$u_{slip} = u_d - u_c$$

II.3 Turbulent Two-Phase Flow Modelling

When the characteristic Reynolds number (Re) of the two-phase mixture under investigation becomes high, the flow transitions and become turbulent. The influence of the turbulence on the flow characteristics (mixing, particle dispersion, pressure drop etc.) are usually significant and warrant the use of a turbulence model.

In order to model fluid flow turbulence, the Euler-Euler Model, Turbulent Flow model uses the k-ε turbulence model. This is realized by solving transport equations for the kinetic energy k (m^2/s^2) and the dissipation rate of turbulent kinetic energy ε (m^2/s^3).

The interface includes the possibility to model the turbulent flow of the two-phase mixture, or to solve for turbulent flow of each phase separately. In the former case one set of k-ε equations are solved, while in the latter two sets of k-ε equations are solved for, one for each phase.

Mixture turbulence assumes that the turbulence effects on the both continuous and dispersed phase can be modelled by solving for the turbulence of the resulting two-phase mixture. Here this is done using a two-equation k-ε model where the transport of turbulence quantities is based on based on the mixture velocity

$$\boldsymbol{u_m} = \frac{\phi_c \rho_c \boldsymbol{u_m} + \phi_d \rho_d \boldsymbol{u_m}}{\rho}$$

And a volume averaged mixture viscosity

$$\boldsymbol{\mu_m} = \phi_c \mu_C + \phi_d \mu_D$$

This implies that the model is appropriate for flows where the relaxation time of the dispersed particles (the time scale on which particles react to changes in the carrier fluid velocity) is not significantly different to the time scale of the turbulence. It is also appropriate for stratified flows, where the mixture mainly consists of one of the phases.

Setting the **Two-phase turbulence** interface property to **Mixture**, the turbulence of the two-phase flow is modelled by solving the following **k** and **ε** equations:

$$\rho \frac{\partial k}{\partial t} + \rho u_m \,.\, \nabla k = \nabla \,.\left(\left(\mu_m + \frac{\mu_T}{\sigma_k}\right) \nabla k\right) = p_k - \rho\varepsilon \qquad (\text{II} - 21)$$

$$\rho\frac{\partial\varepsilon}{\partial t}+\rho u_m\,.\nabla\varepsilon=\nabla\,.\left(\left(\mu_m+\frac{\mu_T}{\sigma_\varepsilon}\right)\nabla\varepsilon\right)=C_{\varepsilon_1}\frac{\varepsilon}{K}p_k-c_{\varepsilon 2}\rho\frac{\varepsilon^2}{k} \qquad (\mathrm{II}-22)$$

The equations correspond to the standard two-equation k-ε model including realizability constraints.

The production term is defined accordingly as

$$p_k{=}\mu_T\left(\nabla u_m{:}\,(\nabla u_m+(\nabla u_m)^T)-\tfrac{2}{3}(\nabla.\,u_m)^2\right)-\tfrac{2}{3}\rho k\nabla.\,u_m$$

And the resulting turbulent viscosity is defined as

$$\mu_T=\rho C_\mu\frac{k^2}{\varepsilon}$$

Where $C_\mu$is a model constant. The viscous stress tensors for the phases are hence defined as

$$\tau_c{=}(\mu_C+\mu_T)\left(\nabla u_c+(\nabla u_c)^T-\tfrac{2}{3}(\nabla.\,u_c)I\right)-\tfrac{2}{3}\rho_c kI$$

$$\tau_d{=}(\mu_D+\mu_T)\left(\nabla u_d+(\nabla u_d)^T-\tfrac{2}{3}(\nabla.\,u_d)I\right)-\tfrac{2}{3}\rho_d kI$$

Assuming mixture turbulence, the transport equation for the volume fraction is:

$$\frac{\partial}{\partial t}(\,\phi_d)+\nabla\,.(\,\phi_d\,u_d)=\nabla\,.\left(\,D_{m,d}\,\nabla\phi_d\right) \qquad (\mathrm{II}-23)$$

Here the dispersion of the particulate phase by the turbulent fluctuations is modelled using a gradient-based hypothesis. The turbulent dispersion coefficient is defined from the turbulent viscosity of the two-phase mixture in the manner of

$$D_{m,d}=\frac{\mu_T}{\rho\sigma_T}$$

Where $\sigma_T$is a turbulent particle Schmidt number (dimensionless).

The default values of the dimensionless parameters using the Mixture Two-phase turbulence model are [CFD Module User's Guide COMSOL].

Table (II - 2): constants

CONSTANT	VALUE
C_μ	0.09
σ_ε	1.3
σ_k	1.0
β	5.2
σ_T	0.35
$C_{\varepsilon 1}$	1.44
$C_{\varepsilon 2}$	1.92
k	0.41

Chapter III : Results and Discussion

III.1 The geometries

A complicated 3D CAD drawing is usually not the best starting point for the modelling process. A 2D representation of a cross section of the geometry can give valuable initial estimates of the flow field that can be used when setting up the full 3D model. For example, you might be able to determine the pressure variations and the nature of the flow, or whether or not a turbulence model is needed. This provides information about where in the final geometry the most amount of 'change' occurs, if a more advanced fluid-flow model and/or better resolution is required, and what parts of the modelling process are more sensitive than others. Simplifying the geometry reduces the simulation time. Making use of symmetry planes can cut down the geometry to one half or even less of the original size. Rounding-off corners is another way to reduce mesh resolution. Resolving small geometric parts requires a fine mesh, but the parts themselves can have a negligible effects on the fluid field as a whole**.** [CFD Module User's Guide COMSOL].

The geometric figure in this study is a rectangle as shown in the figure below. 5m ×1m ×1m (length, width, and height, respectively). This is what the test section looks like in a wind tunnel.

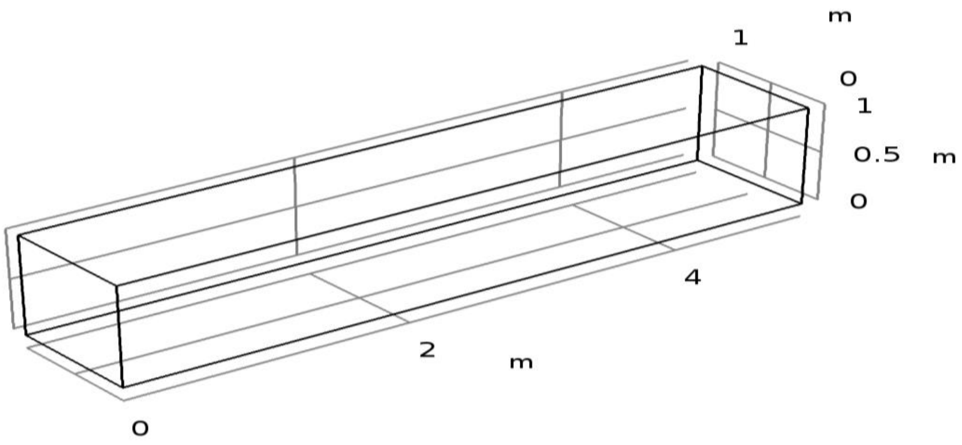

Figure (III - 1): Geometries of wind tunnel

III.1.1 Configuration

In this study, we worked on the velocity change u_c (08-10-12-14. (m/s)) and every time we observe and study continuous phase u_c (m/s) and dispersed phase u_d (m/s) velocity changes, as well as the sand concentration(phid).

As for the other characteristics, they are fixed in each experiment, and they are as in the following table:

Table (III - 1): initial conditions [COMSOL Multiphysics Report date].

Description	**Value**
Velocity field, continuous phase, x component	0.001 (m/s)
Velocity field, continuous phase, y component	0 (m/s)
Velocity field, continuous phase, z component	0 (m/s)
Velocity field, dispersed phase, x component	0.001(m/s)
Velocity field, dispersed phase, y component	0 (m/s)
Velocity field, dispersed phase, z component	0 (m/s)
Pressure	1[atm]
Turbulent kinetic energy, mixture	ee.kinit (m^2/s^2)
Turbulent dissipation rate, mixture	ee.epinit ε (m^2/s^3)
Volume fraction, dispersed phase	0.0001

Table (III - 2): Materials [COMSOL Multiphysics Report date].

Description	**Value**
Continuous phase	Material: Air (mat1)
Dispersed phase	Domain material(sand ston)
Density, continuous phase	From material
Dynamic viscosity, pure continuous phase	From material
Density, dispersed phase	User defined
Density, dispersed phase	2600 kg/m^3
Diameter of particles/droplets	200e-6[m]
Viscosity model	Calculate from mixture viscosity

Description	Value
Mixture viscosity model	User defined
Dynamic viscosity	ee.muinit
Drag model	Schiller - Naumann
Solid pressure model	No solid pressure
Mixing length limit	Automatic
Temperature	User defined
Temperature	293.15[K]

III.1.2 The Mesh

The mesh used in a fluid flow simulation depends on the fluid flow model and on the accuracy required in the simulation. A fluid flow model can inherently require a fine resolution in order to converge, even though the results might not require a correspondingly high accuracy. In such cases, it can be a good idea to change the fluid flow model. An example is the low-reynolds number *k-ε* model, which gives a very accurate description of the flow near solid walls, but requires a very fine mesh there. In many cases, the standard *k-ε* model with wall functions can deliver an accurate enough result at a much lower computational cost. In other cases, the requirement of accuracy in the results can limit the maximum element size. [CFD Module User’s Guide COMSOL].

The mesh of this study:

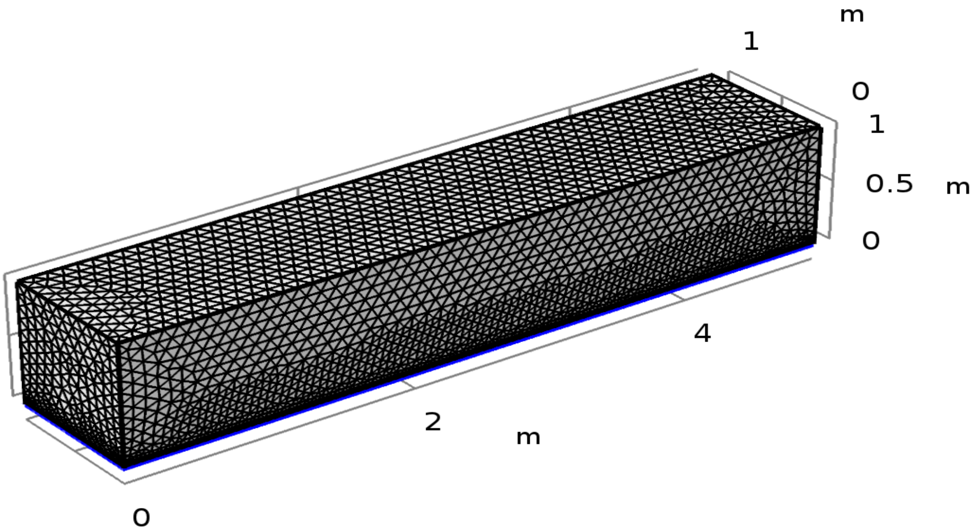

Figure (III - 2): Scheme of the mesh used in 3D

a) The Details of the Mesh

Table (III - 3): Mesh Details [COMSOL Multiphysics Report date].

Description	Value
Minimum element quality	0.02945
Average element quality	0.6174
Tetrahedron	117510
Prism	21060
Triangle	9990
Quad	1140
Edge element	416
Vertex element	8

b) Taille (size)

Table (III - 4) : Taille [COMSOL Multiphysics Report date].

Description	Value
Calibrate for	Fluid dynamics
Maximum element size	0.1
Minimum element size	0.03
Curvature factor	0.7
Resolution of narrow regions	0.6
Maximum element growth rate	1.2
Predefined size	Coarse
Number of boundary elements	18588
Number of elements	198973

III.2 Velocity magnitude, continuous phase u_c (m/s)

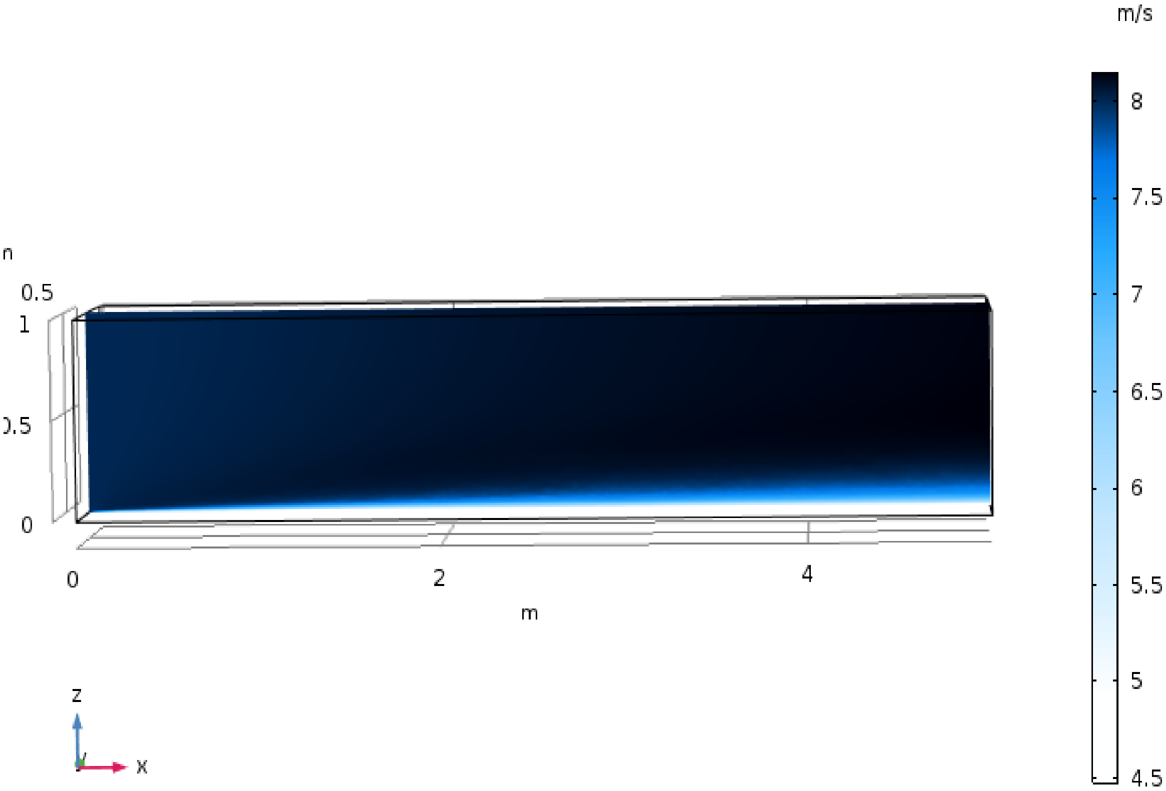

Figure (III - 3): Velocity magnitude, continuous phase u_c=08(m/s).

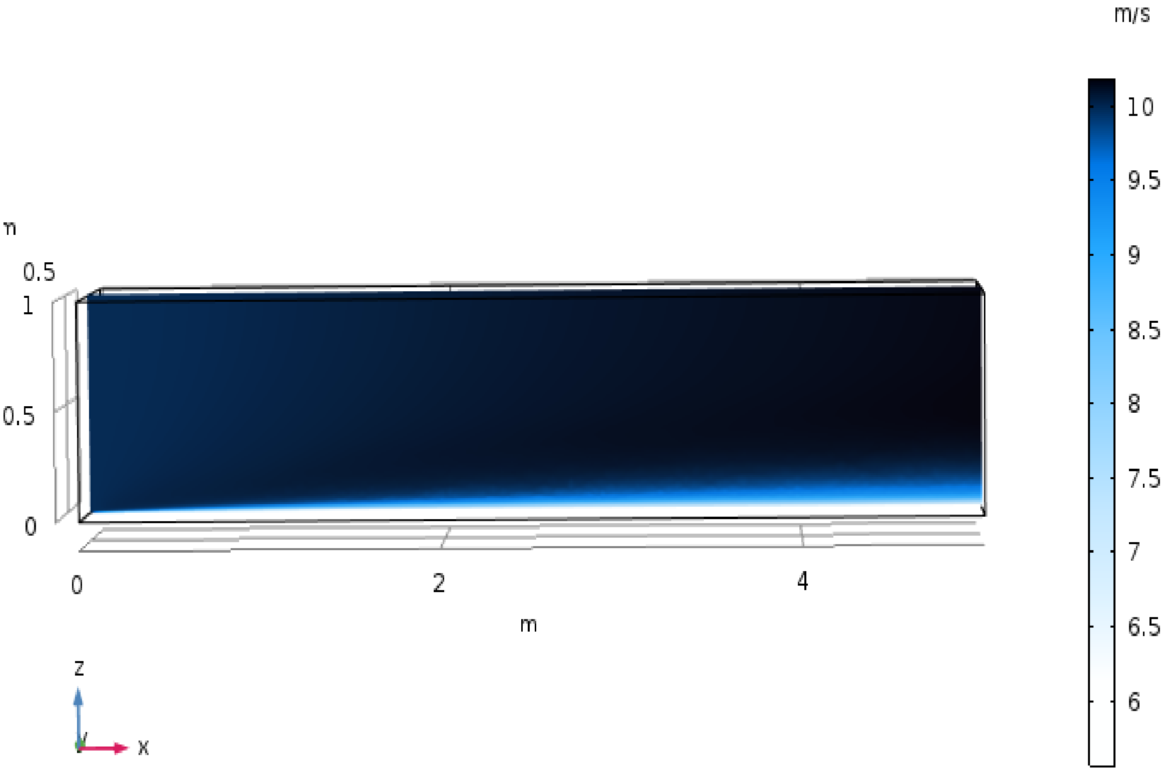

Figure (III - 4): Velocity magnitude, continuous phase u_c=10(m/s)

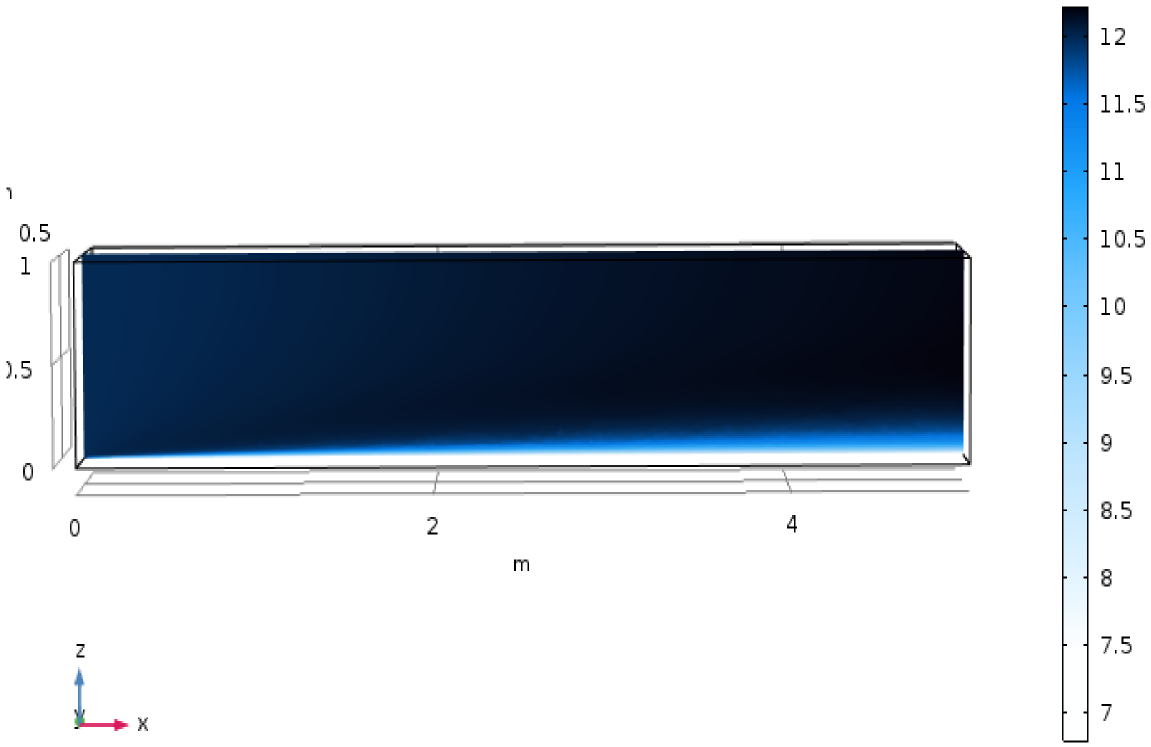

Figure (III - 5): Velocity magnitude, continuous phase u_c=12(m/s)

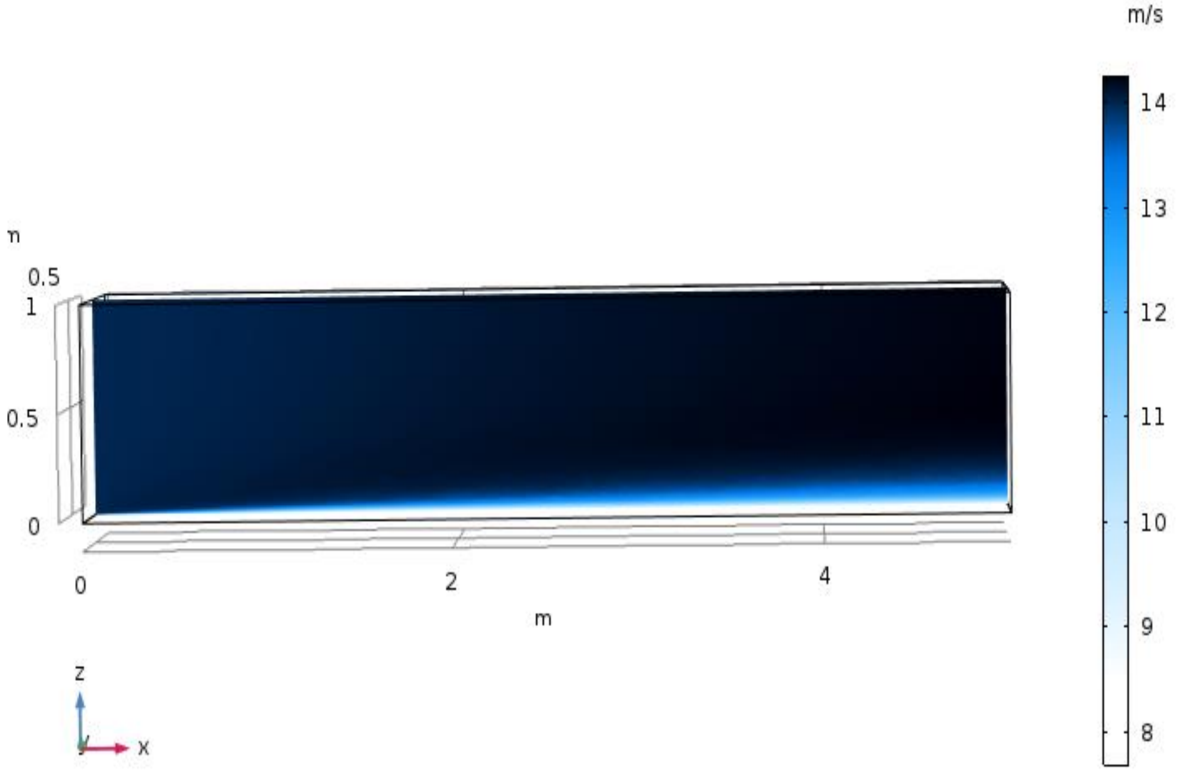

Figure (III - 6): Velocity magnitude, continuous phase u_c=14(m/s)

Figures ((III - 3) to (III - 6)) represents the amount of velocity variance, continuous phase u_c(m/s) inside the wind tunnel.

Dark blue from the beginning to the end of the wind tunnel represents the maximum speed in each case.

At two meters from the beginning of the tunnel to its end, we observed a gradual appearance of white and blue at a height of less than 0.2m, indicating a decrease in velocity.

We found a difference in the minimum velocity of each tunnel and this is according to the velocity of the air entering the tunnel for each case, that is, the higher the air velocity, the higher the minimum velocity at the end and bottom of the tunnel. (Figure (III - 11)) shows the results in more detail.

III.3 Velocity magnitude, dispersed phase u_d (m/s)

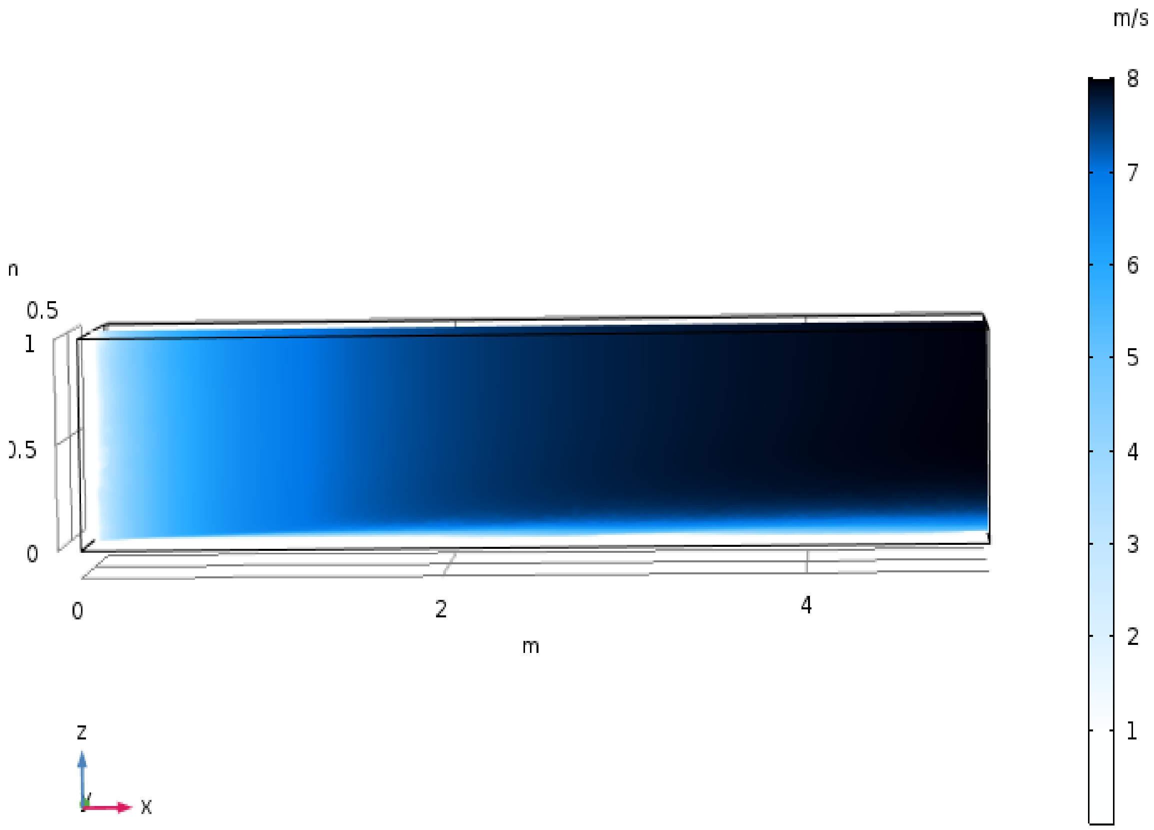

Figure (III - 7): Velocity magnitude, dispersed phase u_d=08(m/s).

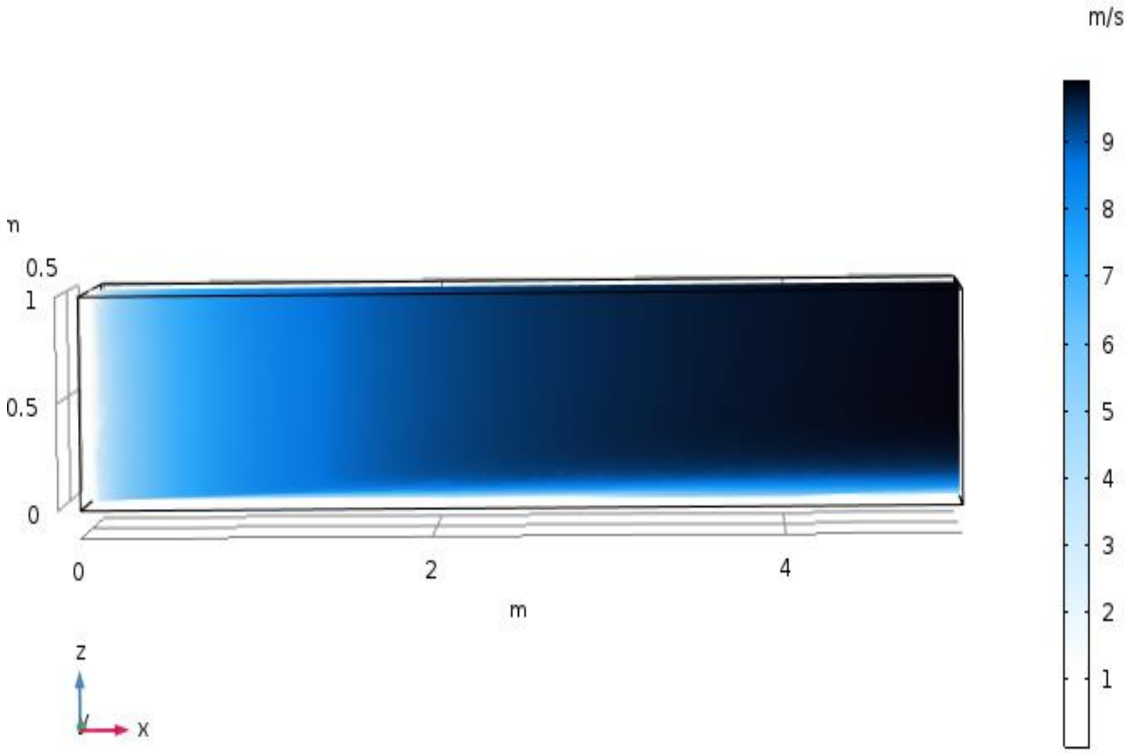

Figure (III - 8): Velocity magnitude, dispersed phase u_d=10(m/s)

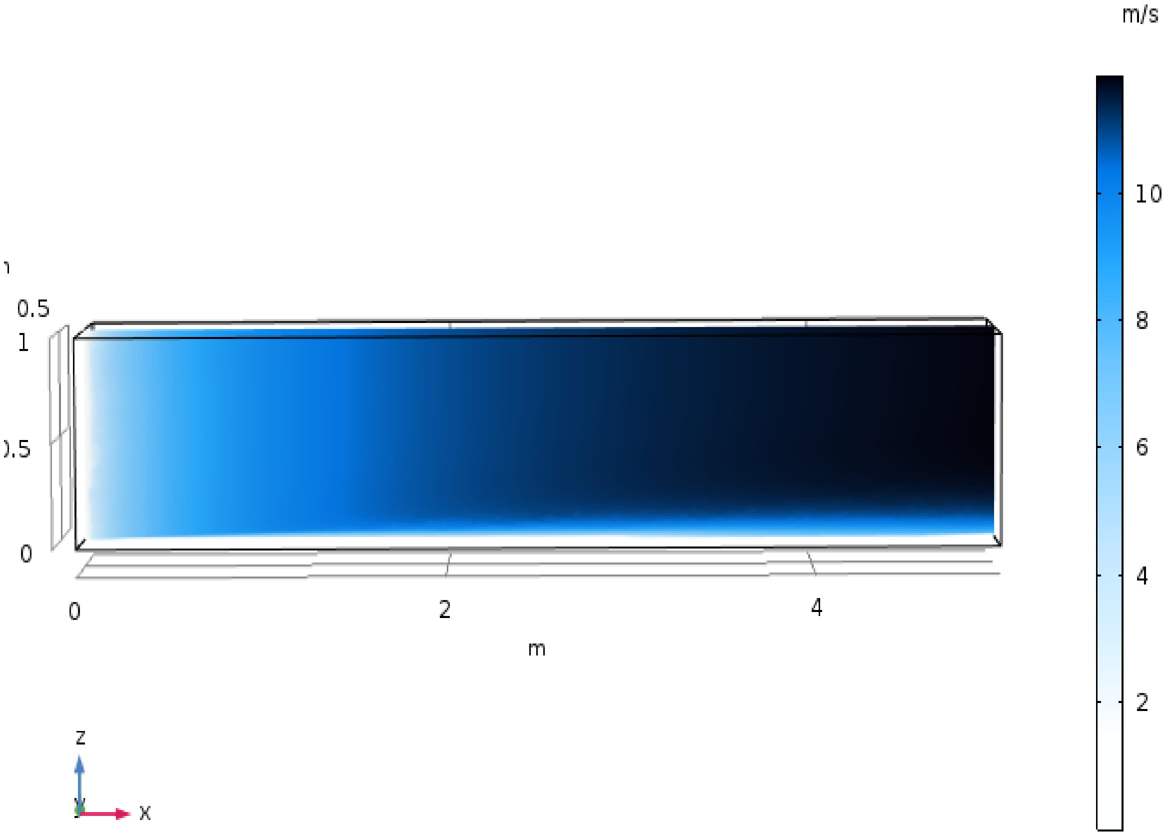

Figure (III - 9): Velocity magnitude, dispersed phase u_d=12(m/s).

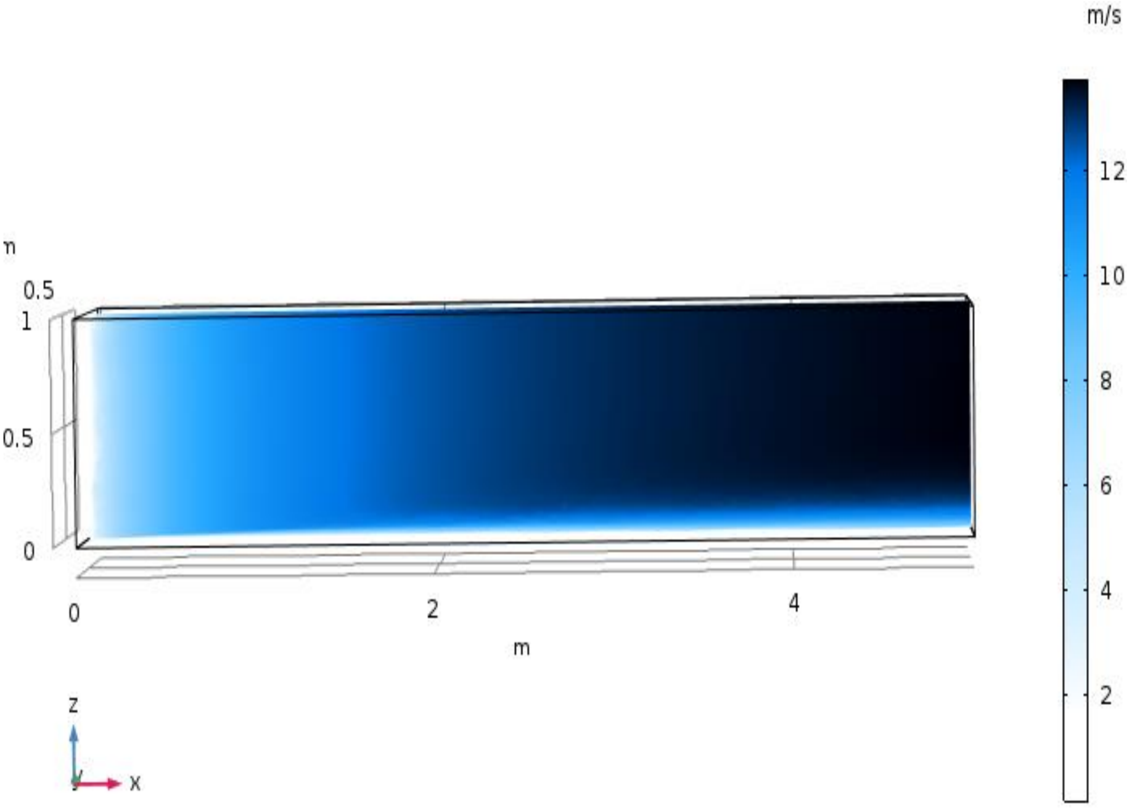

Figure (III - 10): Velocity magnitude, dispersed phase u_d=14(m/s)

Figures ((III - 7) to (III - 10)) represent the velocity-scaling change, dispersive phase u_d(m/s) within the wind tunnel.

From the beginning of the wind tunnel to its end, the color gradually changes from white to dark blue, especially above the height of 0.2m, evidence of an increase in speed.

At 2 m from the beginning of the tunnel, it gradually began to appear white, then blue, until the end of the tunnel, with a height of less than 0.2m, indicating a decrease in the velocity of u_d under the tunnel in each case.

And recording document curves (Figure (III - 11)) .It gives clearer results.

III.4 Comparison between $\mathrm{u_c(m/s)}$and $\mathrm{u_d(m/s)}$:

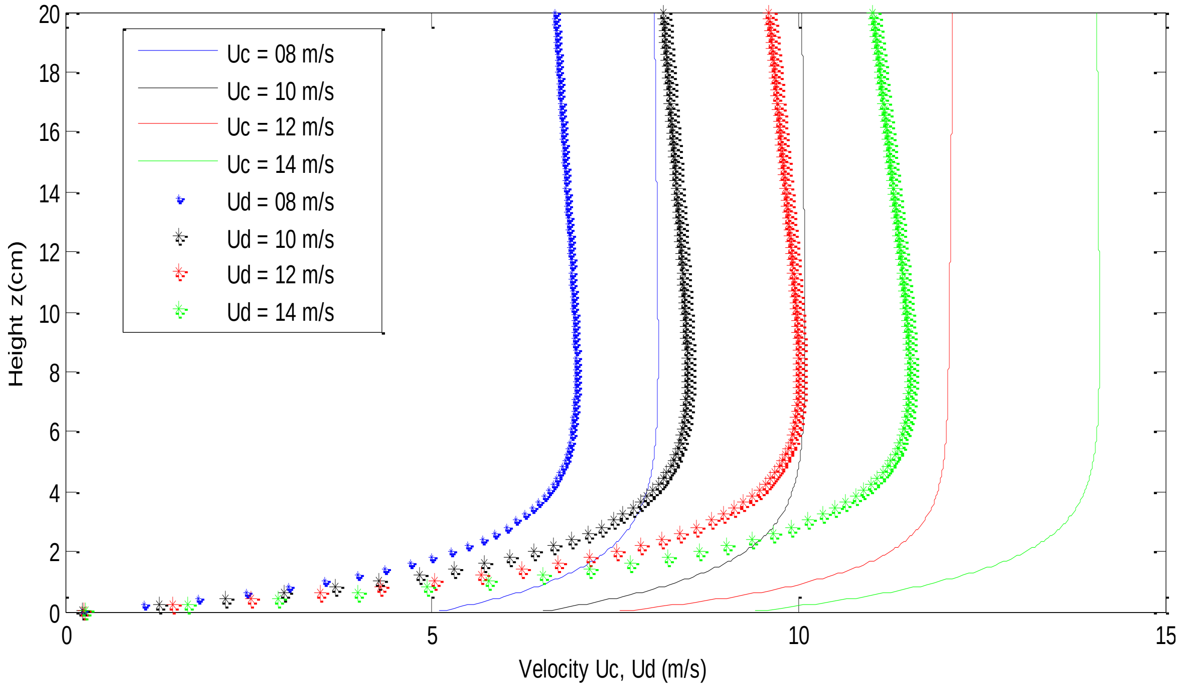

Figure (III - 11): Changes of $u_c(m/s)$ and $u_d(m/s)$ in terms of Height Z (cm)

The figure ((III – 11)) represents the changes of $\mathrm{u_c(m/s)}$ and $\mathrm{u_d(m/s)}$ in terms of Height Z (cm), where $\mathrm{u_c(m/s)}$ is the velocity of Air and $\mathrm{u_d(m/s)}$ is the velocity of Sand and Air together, Notice that all curves are increasing and take an (exp) function shaped function of the second degree with an error ratio comparing the curve and the (exp) in matlab from 93 to 97% : $\mathrm{f(z) = a_1e^{b_1z} + a_2e^{b_2z}}$ (III - 1)

- We also note that the values of $\mathrm{u_c}$ are greater than the values of $\mathrm{u_d}$ in each case.

Example: When Z = 10 cm : $\mathrm{u_c(10) = 8.06\ m/s}$, $\mathrm{u_d(10) = 6.80\ m/s}$

- The percentage change in velocity between $\mathrm{u_c}$and $\mathrm{u_d}$ increases with the speed of

The air in each case, evidence of the interaction between air velocity and the concentration of sand particles.

Example of that:

When:

- $(u_c\,, u_d) = 8\ \text{m/s}$

$$\Delta = \frac{u_c(z)\ -\ u_d(z)}{u_c(z)} \times\ 100 \qquad \text{(III - 2)}$$

With Z = 10 cm $\Rightarrow \Delta_1 = \frac{u_c(10) - u_d(10)}{u_c(10)} \times 100$

$u_c(10) = 8.06\ \text{m/s}\ , u_d(10) = 6.80\ \text{m/s} \quad \Rightarrow \Delta_1 = 15.63\ \%$

- $(u_c\,, u_d) = 10\ \text{m/s}$

$u_c(10) = \ 10.07\ \text{m/s}\ , u_d(10) = 8.32\text{m/s} \quad \Rightarrow \Delta_2 = 17.73\ \%$

- $(u_c\,, u_d) = 12\ \text{m/s}$

$u_c(10) = 12.08\ \text{m/s}\ , u_d(10) = 9.8\ \text{m/s} \quad \Rightarrow \Delta_3 = 18.87\ \%$

- $(u_c\,, u_d) = 14\text{m/s}$

$u_c(10) = 14.09\text{m/s}\ , u_d(10) = 11.26\ \text{m/s} \quad \Rightarrow \Delta_4 = 20\%$

- Si : $\Delta_4 > \Delta_3 > \Delta_2 > \Delta_1$

III.5 Volume fraction, dispersed phase (Phid)

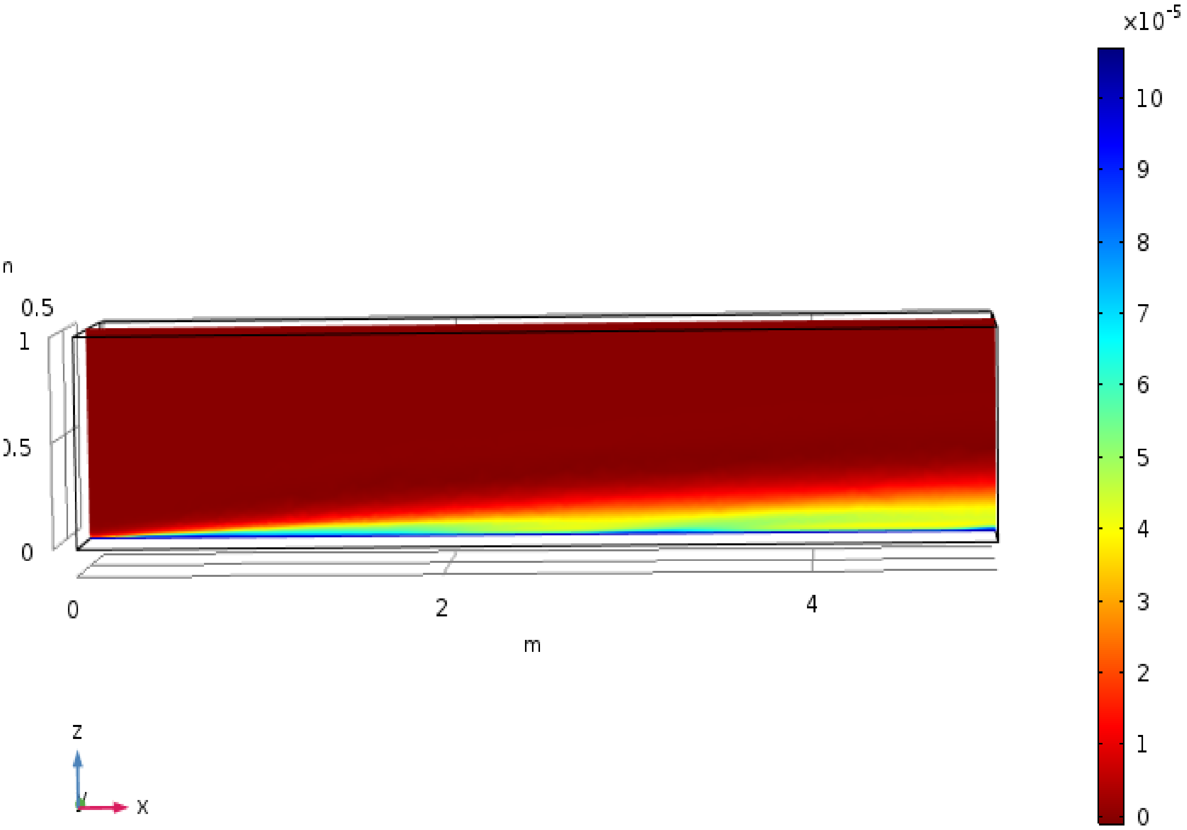

Figure (III - 12): Volume fraction, dispersed phase u_c=08(m/s).

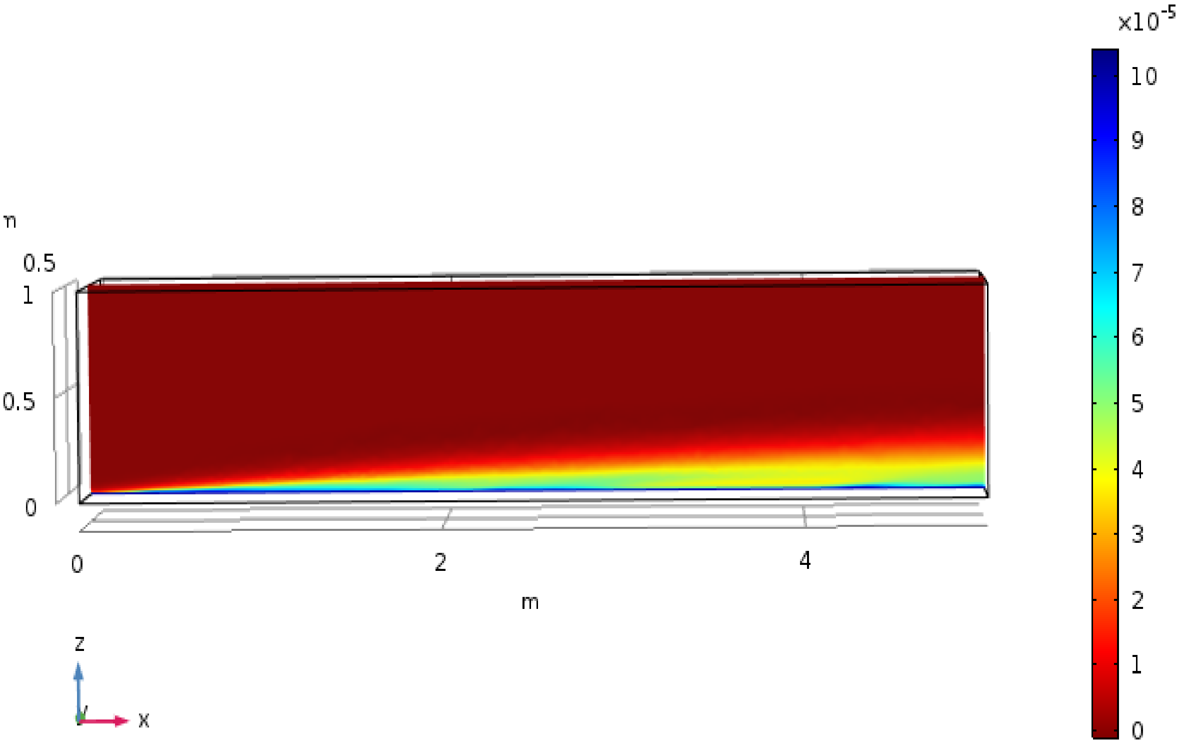

Figure (III - 13): Volume fraction, dispersed phase u_c=10(m/s)

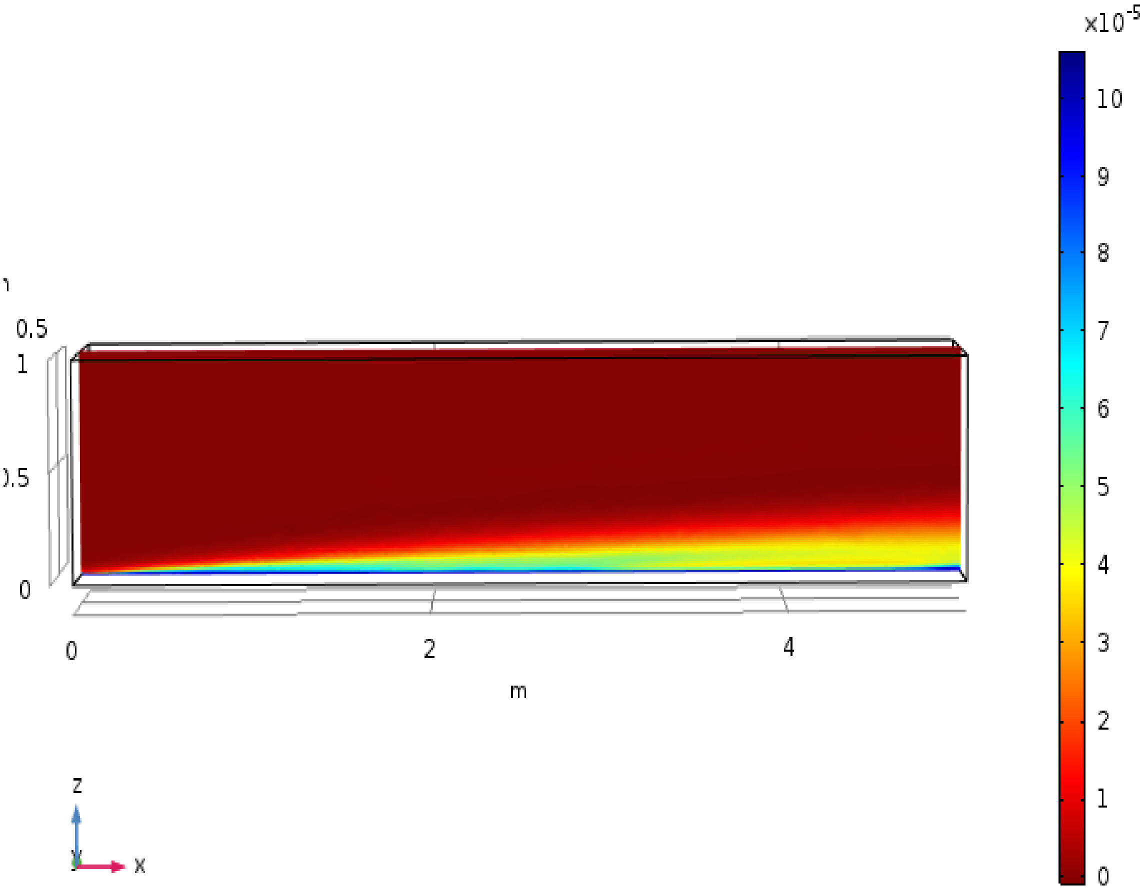

Figure (III - 14): Volume fraction, dispersed phase u_c=12(m/s).

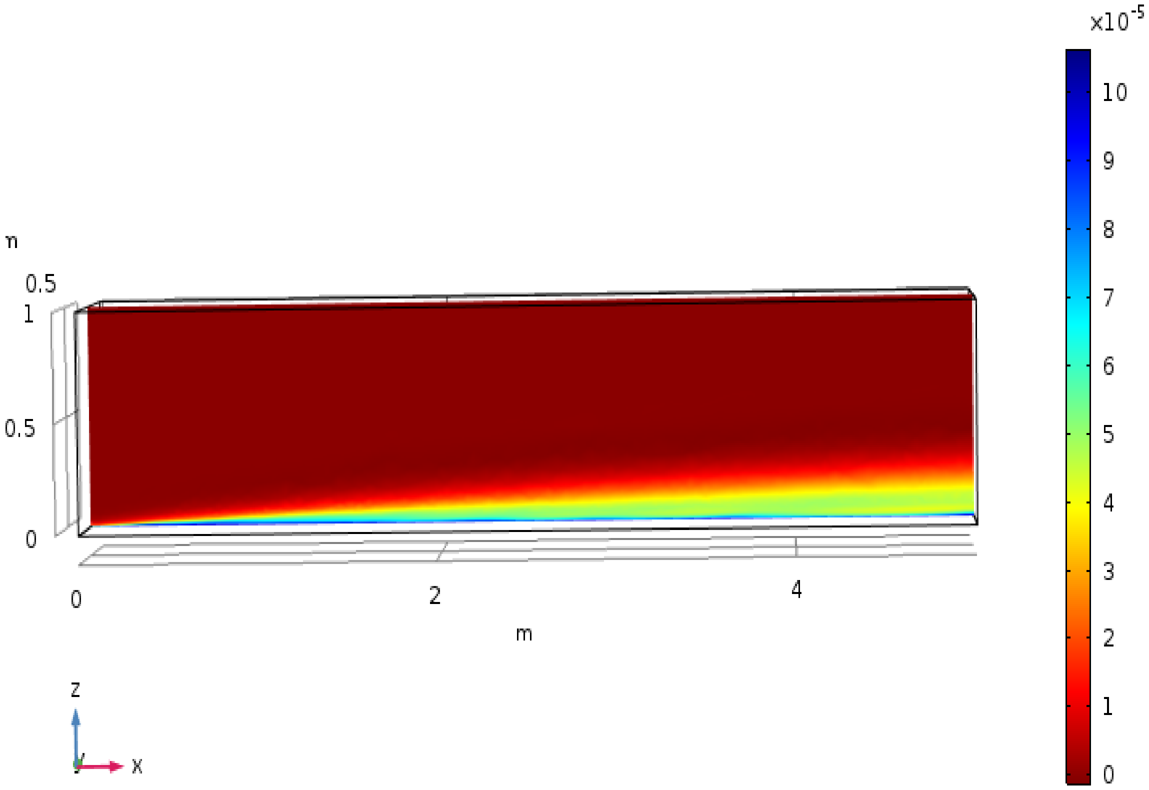

Figure (III - 15): Volume fraction, dispersed phase u_c=14(m/s)

Figures ((III - 12) to (III - 15)) show the change volume fracture, dispersive phase (phid) u_d(m/s) inside the wind tunnel.

The dark red color indicates from the beginning of the wind tunnel to its end, showing sand concentration zero in each case. At a distance of half a meter from the beginning of the tunnel to its end, we notice the appearance of blue, then green, then yellow, then gradually red at a height of less than 0.2 m, which is evidence of an increase in the concentrations of sand grains in each case.

We observed a difference in the maximum concentration value for each tunnel depending on the velocity of the air entering the tunnel, that is, the higher the air velocity, the higher the concentration of sand particles at the end of the tunnel. Figure curves (Figure (III - 16)) and (Figure (III - 17)) the results are clearer.

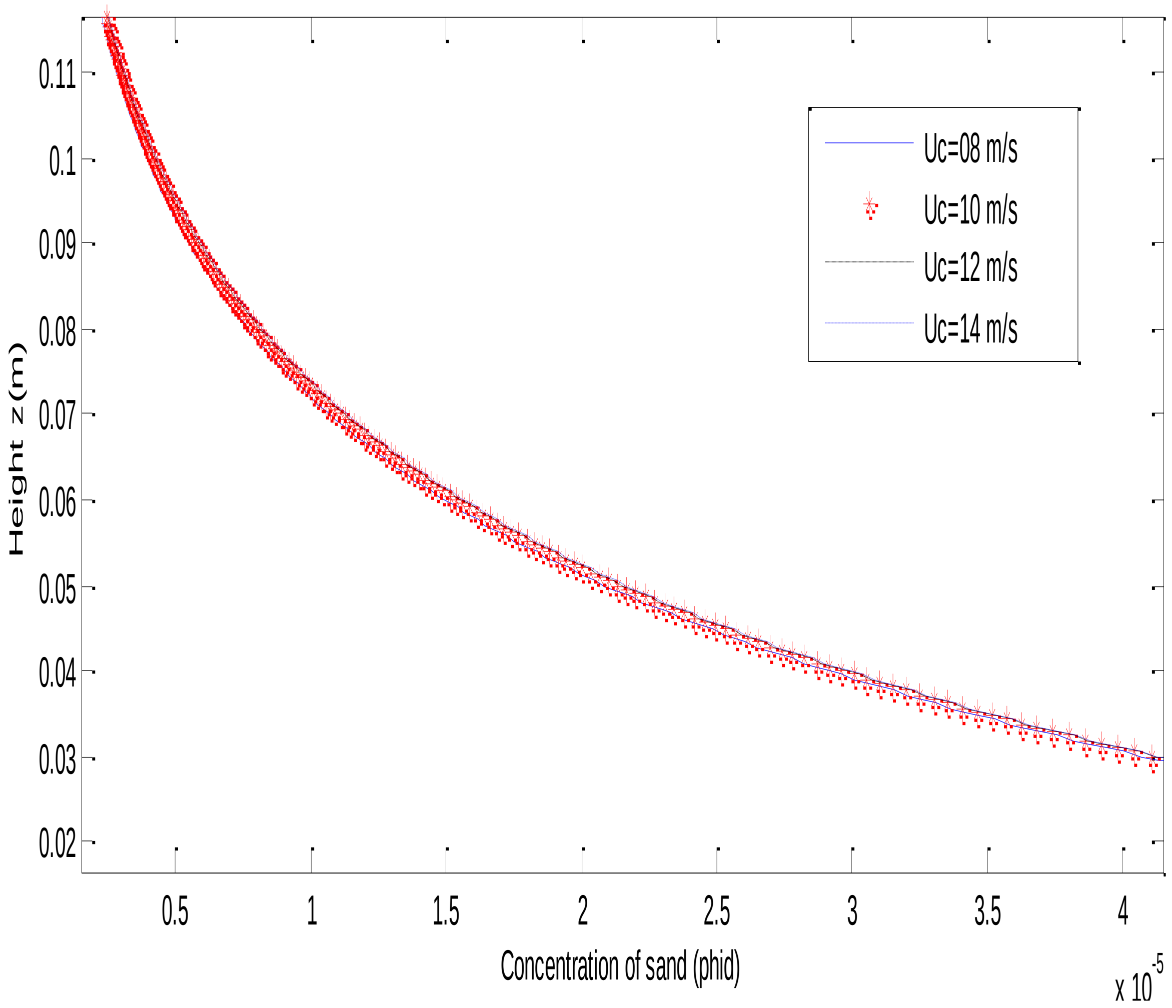

Figure (III - 16): changes velocity $u_c(m/s)$ in terms of concentration of sand (phid) and Height z (m)

The Figure (III -16) represents changes velocity $u_c(m/s)$ in terms of concentration of sand (phid) and Height z (m) where changes in velocity $u_c(m/s)$ take a function of the form (exp) function with an error ratio comparing the curve and the(exp) in matlab from 95 to 99%: $f(z) = a\,e^{-bz}$ (III - 3)

- We note that $u_c(m/s)$ is directly decreasing with Height z (m) with increasing

Concentration of sand (phid) evidence of the effect of the concentration and height of sand particles on the air velocity $u_c(m/s)$.

- By comparing the speeds of $u_c(m/s)$, it becomes clear that concentration of

Sand (phid) is more with an increase u_c(m/s) evidence of the effect of air velocity u_c (m/s) on sand particles.

- When comparing the different speeds presented, we notice that the higher the

u_c (m/s) the higher the sand particles inside the wind tunnel. This refers to the effect of air velocity u_c (m/s) on sand particles by raising it.

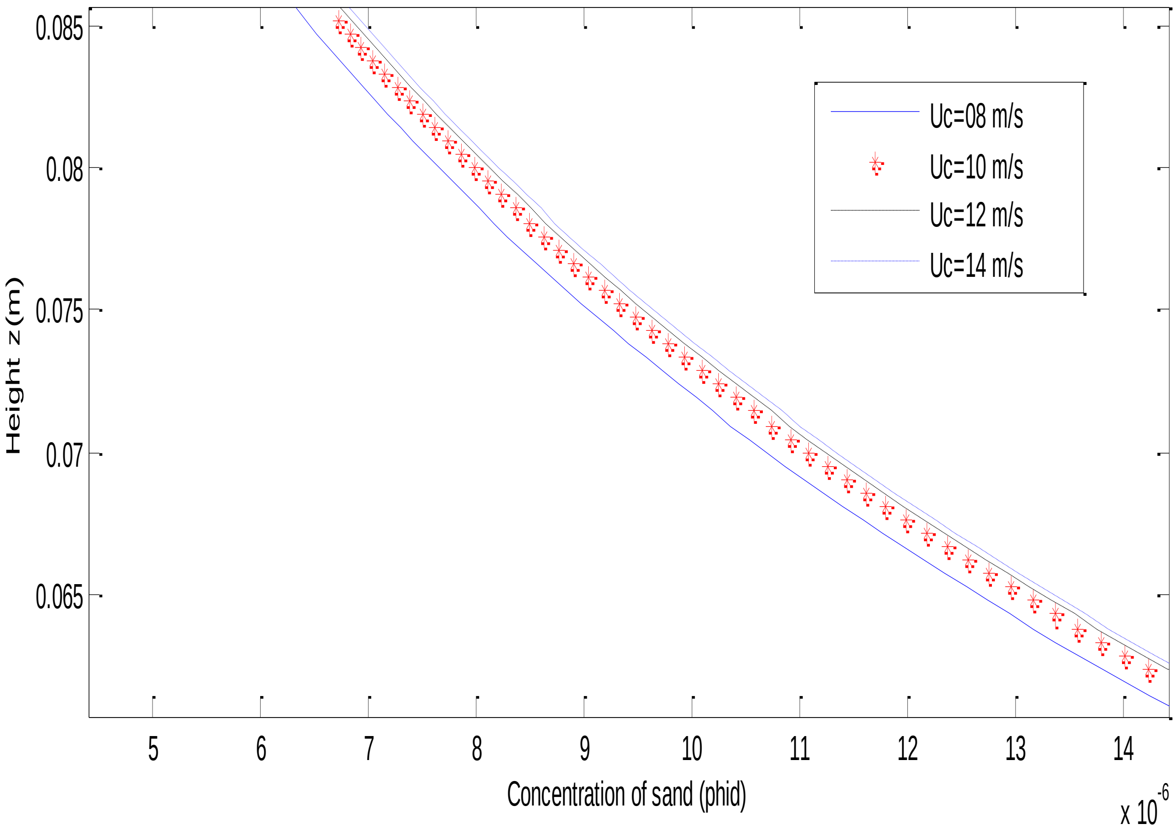

Figure (III - 17): An enlarged section of the Figure ((III - 18))

Conclusion

In this study, we presented a numerical simulation of the concentration of sand particles inside the wind tunnel. Where we conducted this study using “COMSOL Multiphysics ®” through which we chose the Euler-Euler interface .Which uses an average calculation of Navier-Stock equations for each stage on a small size compared to the arithmetic field.

In order to model the turbulent flow of a fluid the Euler interface uses the turbulent flow interface of the turbulent k-ε model. This is done by solving the transport equations for kinetic energy k (m^2/s^2) and the rate of dissipation of turbulent kinetic energy ε (m^2/s^3).

The study was inside a wind tunnel with a certain concentration of sand and every time we changed the speed of the air entering the tunnel,. the results were as follows:

- The higher the wind speed, the greater its effect on the sand grains.
- The decrease in wind speed is due to the gradual increase in sand particles concentration.
- A decrease in wind speed and an increase in sand concentration is evidence of a strong effect and reaction between wind and sand.
- The common forces between wind and sand are the lifting force and the drag force from the wind side and the resistance force of the sand particles.
- The height of sand grains depends on their size and wind speed.
- Wind resistance due to the size and mass of sand grains.

Ultimately, such research remains as the turbulent coefficient of dispersion$D_{m,d}$, change in particle diameter, put an obstacle to the flow, Climate effect from one region to another (humidity) ... etc.

Bibliography

Anderson, R. S., & Hallet, B. 1986. Sediment transport by wind: toward a general model. *Bull.Geol. Soc. Am.* 97, 523–535

Anderson, R. S. 1987a. Eolian sediment transport as a stochastic process: the effects of a fluctuating Wind on particle trajectories. *J. Geol.* 95, 497–512.

Anderson, R. S. 1987b. A theoretical model for aeolian impact ripples. *Sedimentology* 34, 943–956.

Barndorff-Nielsen, O. E., Blaesild, P., Jensen, J. L., & Sørensen, M. 1985b. The fascination ofsand. In A. C. Atkinson & S. E. Fienberg (Eds.), *A celebration of statistics – the ISI centenary volume* (pp. 57–87). New York: Springer.

Bagnold, R. A. 1936. The movement of desert sand. *Proc. R. Soc. London, Ser. A* 157, 594–620.

Bagnold, R. A. 1937b. The transport of sand by wind. *Geogr. J.* 89, 409–438.

Bagold, R. A. 1941. *The physics of blown sand and desert dunes*. London: Methuen.

New York.

Bagnold, R. A. 1973. The nature of saltation and “bed-load” transport in water. Proc. R. Soc.London, Ser. A 332, 473–504.

B.G.M. van Wachem, J.C. Schouten, C.M. van den Bleek, R. Krishna, and J.L. Sinclair, 2001. “Comparative Analysis of CFD Models of Dense Gas-Solid Systems,” AIChE Journal, vol. 47, no. 5, pp. 1035–1051.

Bahari, Muhammad Adnin Mat, 2012. *Design, Construction, and Testing of an Open-loop Low-speed Wind Tunnel*. Diss. UMP,

Chepil, W. S., & Milne, R. A. 1939. Comparative study of soil drifting in the fleld and in a wind tunnel. *Sci. Agric.* 19, 249–257.

Chepil, W. S. 1945a. Dynamics of wind erosion: I. Nature of movement of soil by wind. *Soil Sci.* 60, 305–320.

Chepil, W. S. 1961. The use of spheres to measure lift and drag on wind-eroded soil grains. *Proc.Soil Sci. Soc. Am.* 25, 343–345..

Cui, B., Komar, P. D., & Baba, J. 1983. Settling velocities of natural sand grains in air. *J. Sediment.Petrol.* 53, 1205–1211.

C. Crowe, M. Sommerfeld, and Y Tsuji, *Multiphase Flows with Droplets and Particles*, CRC Press, Boca Raton, 1998.

CFD Module User’s Guide COMSOL.pp31.

CFD Module User’s Guide COMSOL.pp33.

CFD Module User’s Guide COMSOL.pp360-361.

CFD Module User’s Guide COMSOL.pp395-398.

CFD Module User’s Guide COMSOL.pp401-403.

COMSOL Multiphysics Report date.

Cheng, Y., Lien, F. S., Yee, E., & Sinclair, R. (2003). A comparison of large eddy simulations with a standard k–ε Reynolds-averaged Navier–Stokes model for the prediction of a fully developed turbulent flow over a matrix of cubes. Journal of Wind Engineering and Industrial Aerodynamics, 91(11), 1301-1328.pp 06-07.

De Ploey, J. 1980. Some field measurements and experimental data on wind blown sands. In M. de Boodt & D. Gabrieli (Eds.), *Assessment of erosion* (pp. 541–552). Chichester: Wiley.

Draga, M. 1983. Eolian activity as a consequence of beach nourishment – observations at Westerland (Sylt), German North Sea coast. *Z. Geomorph. Suppl. Bd.* 45, 303–319.

Di Clemente, M. et al. "DESIGN, EXECUTION AND NUMERICAL REBUILDING OF SHOCK WAVE BOUNDARY LAYER INTERACTION EXPERIMENT IN A PLASMA WIND TUNNEL." WIND TUNNELS: AERODYNAMICS, MODELS AND EXPERIMENTS: 1 .p,132.

Engelhardt, W. F. von. 1977. The origin of sediments and sedimentary rocks. Sedimentary petrology,Part III. New York: Wiley.

Edoardo Foschi. 2020. Design of a return circuit for an open loop Wind tunnel. ALMA MATER STUDIORUM UNIVERSIT`A DI BOLOGNA.1.

Francis, J. R. D. 1973. Experiments on the motion of solitary grains along the bed of a water stream. *Proc. R. Soc. London, Ser. A* 332, 413–471.

flight.engr.ucdavis.edu/facilities/aeronautical-wind-tunnel/

Green, H. L., & Lane, W. R. 1964. *Particulate clouds: dusts, smokes and mists* (2 ed.). London: Spon

Gillette, D. A., Blifford, I. H., & Fryrear, D. W. 1974. The influence of wind velocity on the size distributions of aerosols generated by the wind erosion of soils. *J. Geophys. Res.* 79,

4068–4075..

Gillette, D. A. 1979. Environmental factors affecting dust emission by wind erosion. In C. Morales (Ed.), *Saharan dust* (pp. 71–91). Chichester: Wiley.

Gillette, D. A. 1981. Production of dust that may be carried great distances. In T. L. Péwé (Ed.),*Desert dust* (pp. 11–26). Geol. Soc. Am. Spec. Pap. 186.

Gerety, K.M.,&Slingerland, R. 1983. Nature of the saltating opulation in wind tunnel experiments with heterogeneous size-density sands. In M. E. Brookfield & T. S. Ahlbrandt (Eds.), *Eolian sediments and processes* (pp. 115–131). Amsterdam: Elsevier.

Gerety, K. M. 1984. *A wind-tunnel study of the saltation of heterogeneous (size, density) sands*.Ph.D. Thesis, Pennsylvania State Univ.

Greeley, R., & Iversen, J. D. 1985. *Wind as a geological process*. Cambridge: Cambridge.

Greeley, R., and J. D. Iversen (1985), *Wind as a Geological Process on Earth, Mars, Venus, and Titan*, Cambridge Univ. Press, New York.

Hunt, J. C. R., & Nalpanis, P. 1985. Saltating and suspended particles over flat and sloping surfaces I. Modelling concepts. In O. E. Barndorff-Nielsen, J. J. Møller, K. R. Rassmussen, & B. B.Willetts (Eds.), *Proceedings of the international workshop on the physics of blown sand* (pp.9–36). Dept. Theoretical Statistics, Institute of Mathematics, Univ. Aarhus, Mem. 8.

H. Enwald, E. Peirano, and A.-E. Almstedt, “Eulerian Two-Phase Flow Theory Applied to Fluidization,” Int. J. Multiphase Flow, vol. 22, pp. 21–66, 1996.

Iversen, J. D., Greeley, R., Marshall, J. R., & Pollack, J. B. 1987. Aeolian saltation threshold: the effect of density ratio. *Sedimentology* 34, 699–706.

Jensen, J. L., & Sørensen, M. 1983. On the mathematical modeling of aeolian saltation. In B. M. Sumer & A. Muller (Eds.), *Mechanics of sediment transport* (pp. 65–72). Rotterdam:Balkema.

Joly, J. 1904. Formation of sand ripples. *Sci. Proc. R. Dublin Soc. N.S.* 10, 328–330.

J. D. Pereira, Wind Tunnels, 2011: Aerodynamics, Models and experiments. Nova Science Publishers, Inc.,

Kármán, T. von. 1937. Turbulence. *J. R. Aeron. Soc.* 41, 1109–1143.

K. Sawada et al 1987.A Numerical Investigation on Wing / Nacelle Interferences of USB Configuration . AIAA Paper87-0455 (in Japanese).

Kok, Jasper F., and Nilton O. Renno. 2009. "A comprehensive numerical model of steady state saltation (COMSALT)." *Journal of Geophysical Research: Atmospheres* 114.D17.

Kok, J.F., Parteli, E.J.R., Michaels, T.I. and Karam, D.B..., 2012. The physcis of wind-blown sand and dust. Rep. Prog. Phys. Vol. 75, Doi:10.1088/0034-4885/75/10/106901.

Lumley, J. L., & Panofsky, H. A. 1964. *The structure of atmospheric turbulence*. New York:Wiley.

McGee, W. J. 1908. Outlines of Hydrology. *Bull. Geol. Soc. Am.* 19, 193–220.

Middleton, G. V.,&Southard, J. B. 1978. *Mechanics of sediment movement*. Binghamton, S.E.P.M.short course No. 3.

Mitha, S., Tran, M. Q.,Werner, B. T., & Haff, P. K. 1986. The grain-bed impact process in Aeolian saltation. *Acta Mech.* 63, 267–278.

Nickling, W. G. 1983. Grain-size characteristics of sediment transported during dust storms.*J. Sediment. Petrol.* 53, 1011–1024.

Nalpanis, P. 1985. Saltating and suspended particles over flat and sloping surfaces. II. Experiments And numerical simulations. In O. E. Barndorff-Nielsen, J. T.Møller, K. R. Rasmussen, & B. B. Willetts (Eds.), *Proceedings of the international workshop on the physics of blown sand* (pp.37–66). Dept. Theoretical Statistics, Institute of Mathematics, Univ. Aarhus, Mem. 8.

Nickling, W.G. and Davidson-Arnott, R.G.D., 1990. Aeolian sediment transport on beaches and coastal dunes. Proc. Canadian Symposium on coastal sand dunes.

Owens, J. S. 1927. The movement of sand by wind. *Engineer* **143**, 377.

Owen, P. R. 1964. Saltation of uniform grains in air. *J. Fluid Mech.* **20**, 225–242

Owen, P. R. 1980. *The physics of sand movement*. Trieste: International Centre for Theoretical Physics. (Lecture Notes, Workshop on physics of flow in deserts).

Pye, K. 1987. *Aeolian dust and dust deposits*. London: Academic Press.

Pye, Kenneth, and Haim Tsoar, 2008. *Aeolian sand and sand dunes*. Springer Science & Business Media.pp. 113–124.

Sharp, R. P. 1964. Wind-driven sand in Coachella Valley, California. *Bull. Geol. Soc. Am.* **75**,785–804.

Shao, Y. P. (2000), *Physics and Modelling of Wind Erosion*, Kluwer Acad., Dordrecht, Netherlands

Tsuchiya, Y. 1970. Successive saltation of a sand grain by wind. *Proc. 2th Conf. Coastal Eng.* **1**, 1417–1427.

Tsoar, H., & Pye, K. 1987. Dust transport and the question of desert loess formation. *Sedimentology* **34**, 139–153.

Ungar, J. E., & Haff, P. K. 1987. Steady state saltation in air. *Sedimentology* **34**, 289–299.

Valance, A., Rasmussen, K.R., Moctar, A.O.E and Dupont, P., 2015. The physics of aeolian sand transport. Comptes Rendus Physique, Elsevier Masson, Vol. 16 (1), 1-13. Doi: 10.1016/j.crhy.2015.01.006 .

Van Rijn, Leo C, 2018. "Aeolian transport over a flat sediment surface." *Leovanrijn-Sediment: Blokzijl, the Netherlands.* Pp.1-3.

Williams, G. 1964. Some aspects of the eolian saltation load. *Sedimentology* 3, 257–287.

White, B. R., & Schulz, J. C. 1977. Magnus effect in saltation. *J. Fluid Mech.* 81, 497–512.

White, B. R. 1982. Two-phase measurements of saltating turbulent boundary-layer flow. *Int. J.Multiphase Flow* 8, 459–473.

Willetts, B. B. 1983. Transport by the wind of granular material of different grain shapes and densities. *Sedimentology* 309, 669–679.

Willetts, B. B., & Rice, M. A. 1985a. Inter-saltation collisions. In O. E. Barndorff-Nielsen, J. T.Møller, K. R. Rasmussen, & B. B. Willets (Eds.), *Proceedings of the international workshop on the physics of blown sand* (pp. 83–100). Dept. Theoretical Statistics, Institute of Mathematics,Univ. Aarhus, Mem. 8.

Willetts, B. B., & Rice, M. A. 1986a. Collisions in aeolian saltation. *Acta Mech.* 63, 255–265.

www.edibon.com/en/computer-controlled-aerodynamic-tunnel-300-x-300-mm

Y. Matsuo et al 2010.: The Numerical Simulator III Acquisition and Installation , its Operation , Performance Evaluation , and the Critical Issues to the Next Generation Supercomputing . JAXA - RR - 10-005 (in Japanese).

Y. Matsuo, 2017 : Numerical Wind Tunnel : History and Evolution of Supercomputing FUJITSU Sci . Tech . J. , Vol . 53.pp.

Zingg, A. W. 1953a. Wind tunnel studies of the movement of sedimentary material. *Proceedings of the 5th Hydraulics Conf. Bull.* **34**, 111–135. Iowa City: Inst. of Hydraulics.

Zingg, A. W. 1953b. Quelques caractéristiques du mouvement éolien du sable par le processus de saltation. *Éditions du Centre National de la Récherche Scientifique* **13**, 197–208.